NASA DEVELOP National Program
Massachusetts – Boston

Spring 2024

Alaska Ecological Conservation

Using NASA Earth Observations to Identify Recent Changes in River Ice Phenology and Its Impacts on Caribou Migration

DEVELOP Technical Report

March 29th, 2024

Christian Sarro (Project Lead)
Levi Mitchell
Mahnoor Naeem
Ben Silver

Advisor:
Dr. Cédric Fichot, Boston University (Science Advisor)

Lead:
Madison Arndt (Massachusetts – Boston)

1. Abstract
Each fall, caribou (*Rangifer tarandus*) in the Western Arctic Herd migrate hundreds of kilometers across northwestern Alaska to acquire seasonal resources and reach wintering grounds. Various rivers intersect migration paths, and caribou can only cross over open water or high-ice extents but are unable to cross rivers in stages of partial freezing. Recent temperature increases in Alaska can alter the timing and duration of ice formation periods, impeding migratory patterns. The Massachusetts NASA DEVELOP team partnered with the National Park Service in Alaska to detect river ice onset dates and formation periods using Landsat 8 Operational Land Imager and Landsat 9 Operational Land Imager-2, Sentinel-1 C-band Synthetic Aperture Radar and Sentinel-2A/B MultiSpectral Instrument imagery in Google Earth Engine. This feasibility analysis measured ice coverage using the Normalized Difference Infrared Index, Relative Difference River Ice, and Vertical-Vertical/Vertical-Horizontal backscatter values based on the spectral and surface characteristics of rivers. The team produced annual freezing timelines, time series plots, and maps at three river stretches to analyze river ice phenology changes. Radar imagery assessed ice coverage more accurately, while optical imagery better identified ice onset dates. Meanwhile indices were unable to robustly establish ice formation thresholds across the study period. These study results can help the National Park Service to better evaluate spatiotemporal migratory shifts and contextualize recent regional caribou declines.

Key Terms

river phenology, *Rangifer tarandus*, caribou, remote sensing, Landsat, Sentinel, NDWI, RDRI

2. Introduction
2.1 Background Information
Rangifer tarandus, commonly known as caribou or wild reindeer, is a keystone species in supporting predators, maintaining vegetation structural integrity, and cycling nutrients throughout the Alaskan tundra (Mowat & Heard, 2023). The Western Arctic Herd (WAH), the largest Alaskan caribou herd, traverse hundreds of kilometers each year across open and coastal tundra areas (Fullman et al., 2017). Migration is integral for maintaining large populations, as it allows caribou to access seasonal resources and calving grounds, raise offspring, and avoid overcrowding (Joly et al., 2021; Nicholson et al., 2016). While spatial and temporal caribou migration patterns have historically been consistent, recent climatological changes have altered these patterns.

Shifting river ice phenology can lengthen fall migration distances because caribou can only cross rivers during periods of open water or when ice cover is complete and sufficiently thick. If migration is lengthened, the herd expends excess energy diverging from established routes, and can arrive at wintering grounds past peak-resource availability (Le Corre et al., 2017; Cameron et al., 2021). Our partner at the National Park Service hypothesizes that changing migratory conditions are contributing to the WAH's two-decade population decline from 490,000 to 164,000. Altered migratory behaviors pose challenges for conservation managers and hunters monitoring caribou movements. Additionally, caribou are integral to the subsistence harvest, culture, and spirituality of Alaskan peoples, many of whom are indigenous (Joly et al., 2021). The ecological and cultural importance of caribou highlights the significance of addressing threats to the species' migration.

This study analyzed how ice phenology affects WAH migration on sections of the Kobuk and Colville rivers (Figure 1). Specific regions of the rivers were designated as areas of interest based on the partner's observations of river sites with high perceived rates of migratory deflection, delays, or tracing behavior. Warming temperatures have delayed river freezing dates in Northwestern Alaska, and researchers hypothesize that the intermediate phase between open water and high-ice extent has increased in duration (Leblond et al., 2016; Brown et al., 2023). We examined imagery from 2017–2023 since Sentinel-2B imagery began in 2017. We also only included images from the fall migration season to capture the full transition from open water to crossable ice.

Remote sensing and river ice detection literature applied both passive and active methods. Previous studies detected ice through optical remote sensing methods using indices and band ratios to successfully distinguish river physical characteristics (water, ice, snow; Li et al., 2021). Li et al. (2021) used a Relative Difference River Ice Index (RDRI) with the red, near infrared, and short-wave infrared bands to distinguish river ice from snow in the Tibetan plateau. Stonevicius et al. (2022) used synthetic aperture radar (SAR) and found that Sentinel-1 SAR backscatter models better detected river ice formation than Sentinel-2 MultiSpectral Instrument (MSI) because SAR imagery penetrates cloud coverage. In the same study, cloud masks with Sentinel-2 MSI imagery misidentified translucent clouds and misclassified pixel spectral reflectance values between cloud and snow (Stonevicicous et al., 2022). In both studies, optical indices and SAR backscatter thresholds varied by region, hydrological and climatological conditions (Li et al., 2021; Stonevicicous et al., 2022).

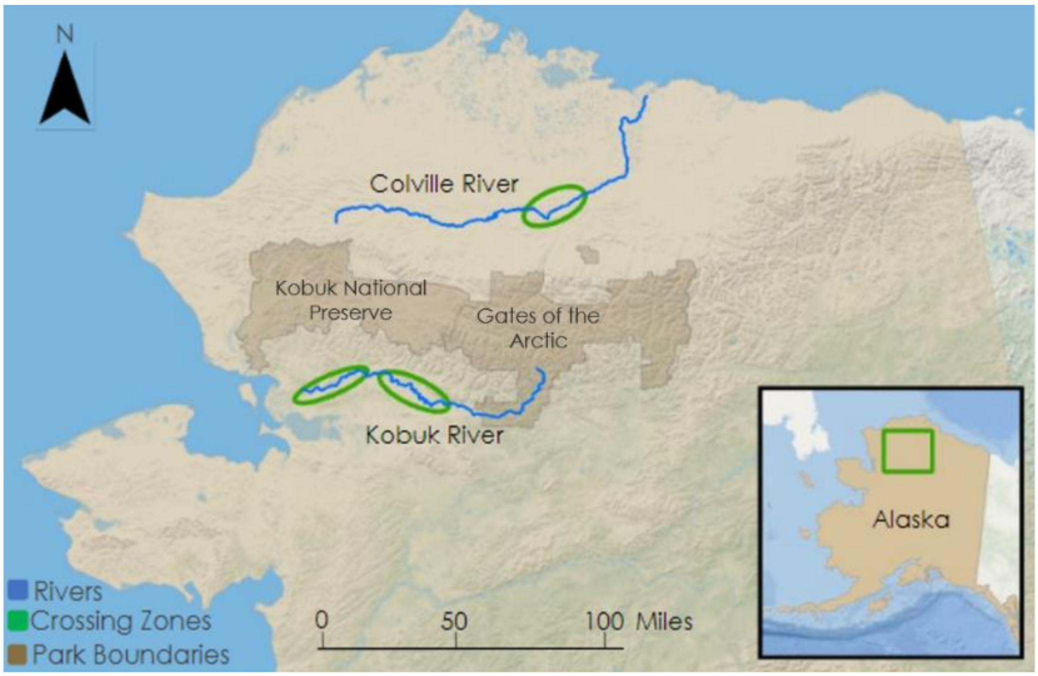

[Basemap Credit: ESRI, GEBCO, Garmin, NaturalVue]

Figure 1. Study area map of Northwestern Alaskan rivers, park boundaries, and caribou crossing areas.

2.2 Project Partners and Objectives

In partnership with the National Park Service – Region 11: Alaska, this study assessed how river ice phenology impacts caribou migration routes. For over two decades, wildlife biologist Dr. Kyle Joly has worked with the Gates of the Arctic and the Yukon-Charley National Parks and Preserves to understand the spatial ecology of caribou in Alaska. Dr. Joly is interested in investigating the timing of river ice formation and how it may be contributing to migration deflections, delays, or tracing patterns of the WAH. To support National Park Service research initiatives, this study analyzed the timing of river ice freeze-up and various stages of ice formation by creating time series maps and plots. Our research explored the feasibility of using remote sensing data to investigate ice phenology on migration patterns under evolving climate conditions. Comparing our results with caribou migration data can help monitor current caribou harvesting initiatives and inform local hunting policy.

3. Methodology

3.1 Data Acquisition

3.1.1 Optical Data Acquisition

This study used publicly accessible spatial data and satellite imagery to analyze river ice formation. The river polygon shapefile was retrieved from the National Hydrography Dataset (NHDPlus) on the United States Geological Survey National Map Viewer (U.S. Geological Survey, 2022). We extracted the names of the Kobuk and Colville Rivers in Northwest Alaska from the dataset and then imported the polygons into Google Earth Engine (GEE). We acquired imagery of the rivers using Landsat 9 Operational Land Imager (OLI)-2, Landsat 8 OLI, Sentinel-2 MSI, and

Sentinel-1 SAR from the GEE Catalog (Table 1). Using Landsat 8 OLI, Landsat 9 OLI-2, and Sentinel-2 MSI satellites, we were able to employ a passive sensor for optical analysis, spectral reflectance bands, and index analyses. Sentinel-2A/B level 1 and level 2 imagery, alongside Landsat 8 OLI and Landsat 9 OLI-2 were used for the annual ice formation time series.

Table 1
Earth observations and datasets used for detecting ice on river surface

Sensor	Resolution	Processing Level	GEE ImageCollection ID
Sentinel-1 C-SAR	5m x 20m	S1 Ground Range Detected	COPERNICUS/S1_GRD
Sentinel-2 MSI A/B	10m, 20m	Level-1C	COPERNICUS/S2_HARMONIZED
Sentinel-2 MSI A/B	10m, 20m	Level-2A	COPERNICUS/S2_SR
Landsat 8 OLI	30m	Level 2 Tier 2 Reflectance	LANDSAT/LC08/C02/T2_TOA
Landsat 9 OLI-2	30m	Level 2 Tier 2 Reflectance	LANDSAT/LC09/C02/T2_TOA

We collected images from September 1st to November 30th to capture the annual period of ice formation in the Colville and Kobuk rivers. While some portions of the rivers did not completely freeze by November 30th, optical imagery was not available on these dates due to the shortening of days in winter in Alaska. Image availability varied site to site, as data for the northern Colville study site ended in mid-October, while the southern Kobuk River continued through early November. We filtered Landsat and Sentinel image collections for each year to only include images with under 30% cloud coverage.

3.1.2 Radar Data Acquisition
We used Sentinel-1 C-SAR satellite data to include an active sensor in the analysis which can produce imagery regardless of cloud cover and thereby provide temporally consistent time series. The SAR sensor aboard Sentinel-1 measured backscatter data used to produce time series plots and maps of the VV and VH band values to show a correlation between backscatter and river ice formation phases. To further substantiate our results, we obtained air temperature data from weather stations near the study rivers such as Kiana, Knifeblade Ridge, and Ambler (MesoWest Fire and Fuels, 2024).

Utilizing SAR, we analyzed backscatter to detect ice formation and filtered Sentinel-1 data to acquire imagery for the fall, specifically from September 1st to November 30th. We then filtered the dataset to only include images with the VV and VH polarizations and the Interferometric Wide instrument mode as they are commonly used for surface analysis. This imagery allowed us to have a more detailed look at the rivers without the interference of clouds.

We georeferenced river polygons at the caribou migration locations identified by the National Park Service. Due to seasonal fluctuations in river flow, volume, and adjacent water bodies, we could not be confident that existing GIS hydrography datasets and base maps accurately depicted river coverage during the study period. Thus, we digitized each river polygon by referencing Sentinel-1 C-SAR radar imagery and the NHDPlus river shapefile. While digitizing, we reduced the transparency of the Senitinel-1 image layer, to allow our polygons to reflect the most recent and accurate shape and flow of the rivers.

3.2 Data Processing
3.2.1 Optical Data Processing
The initial steps for our optical imagery data processing were collecting a mosaic of images then implementing a cloud mask. We generated mosaics annually for each date containing images, and a new image collection was defined from the resulting mosaics. The Sentinel-2 Cloud Probability layer, which approximates the probability of each pixel containing clouds, was filtered to the study period, clipped to the rivers, and joined to the Sentinel-2 imagery. We then masked pixels in each image with a cloud probability greater than 50% to limit cloud interference

on spectral index calculations. Since our mask did not accurately distinguish clouds from snow in the Landsat imagery, we excluded images containing extensive cloud coverage (Figure 2).

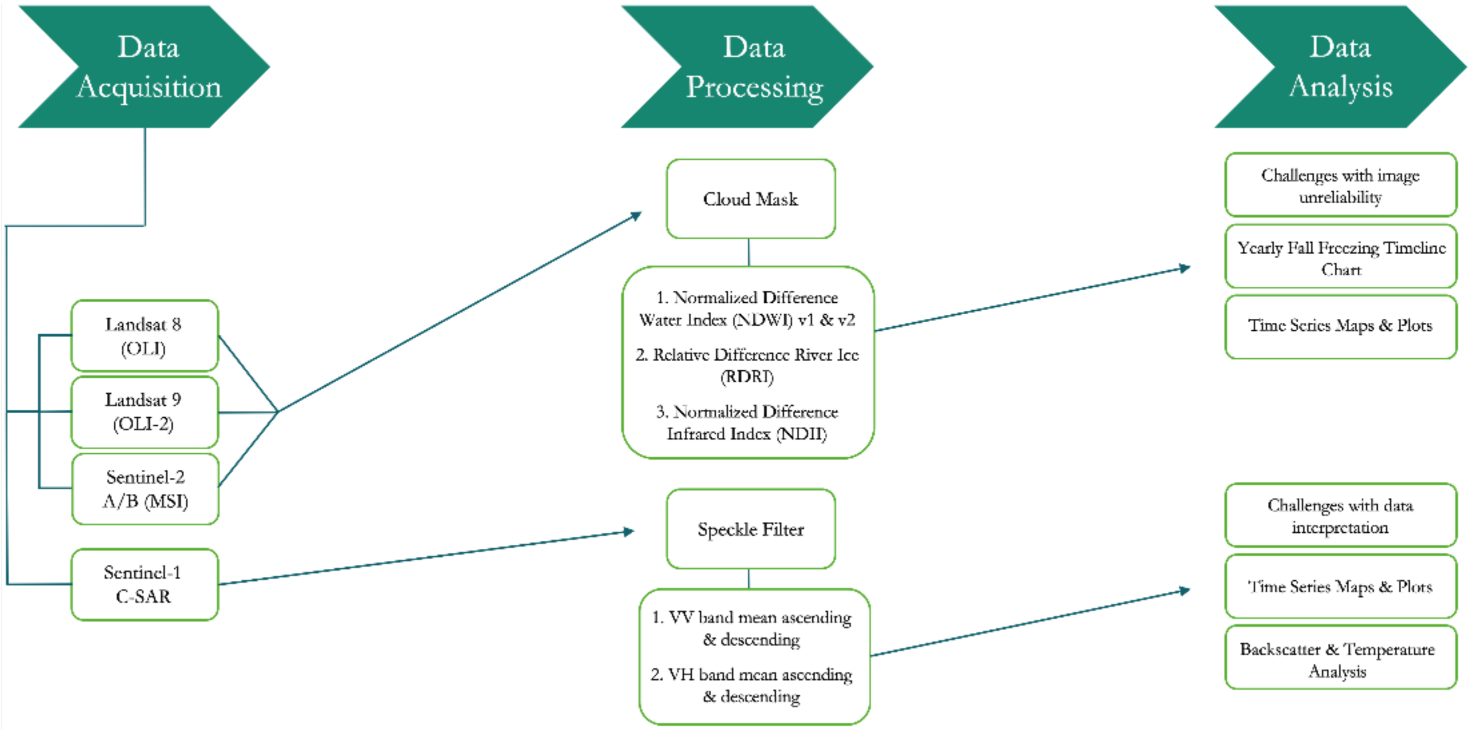

Figure 2. Workflow methodology for data acquisition, processing, and analysis.

The normalized difference water index (NDWI) can be used to determine free-flowing water to construct a time series of yearly freezing (Gao, 1996). For Sentinel-2A/B, Landsat 8, and Landsat 9, the first NDWI equation was computed using the Green and NIR bands (Equation 1 in Table 2). We also implemented a second NDWI index utilizing the short-wave infrared bands (SWIR) using Sentinel-2 and Landsat's Green and SWIR bands (Equation 2 in Table 2). The NDWI value helped distinguish water from ice formation and confirm phases of open water in the time series of yearly freezing.

The RDRI index was presented by Li et al (2021) to determine river ice using its spectral characteristics. RDRI can distinguish between river ice and snow cover by taking the difference in the reflectivity of the red and near infrared (NIR) bands and dividing that by the sum of the reflectivity of the NIR and SWIR bands (Equation 3, Table 2). This index provided an RDRI value per pixel and helped determine river ice coverage for the time series of yearly freezing.

The normalized difference infrared index (NDII) has been used in various ways to detect moisture and land surface water (Ji et al, 2011). The normalized difference function in GEE uses the NIR and SWIR1 (1566–1651 nanometers) for both Sentinel-2 and Landsat data (Equation 4 in Table 2). This yielded an estimate of infrared energy for each pixel within the river shapefile, which is a useful indicator in identifying open water.

Table 2

Index calculations formatted bands and function for optical imagery

Equation #	Index:	Function:
Equation 1	NDWI with NIR	$\frac{Green - NIR}{Green + NIR}$

Equation 2	NDWI with SWIR	$\frac{Green - SWIR1}{Green + SWIR1}$
Equation 3	RDRI	$\frac{Red - NIR}{NIR + SWIR1}$
Equation 4	NDII	$\frac{NIR - SWIR1}{NIR + SWIR1}$

3.2.2 Radar Data Processing
For Sentinel-1 imagery, we first applied a speckle filter to reduce the noise in the imagery. The speckle filter was implemented by performing a spatial filtering operation, computing the mean value of pixels within a circular neighborhood with a radius of 50 meters. This preprocessing step allowed us to work with speckle free images. We then filtered the dataset to only include the VV and VH polarizations (Figure 2). VV backscatter refers to when the radar signal is being transmitted and received vertically, and VH is when the signal is transmitted vertically and received horizontally. These polarizations are often used for spatial analysis.

3.3 Data Analysis
3.3.1 Optical Data Analysis
Using the NDWI, NDII, and RDRI indices, we calculated a mean value through the reducer function to determine the river's condition for each study site, for each day with usable imagery. The index means were analyzed to be used in a time series plot and map. For each index, the image collection means were converted to feature collections, exported to a table, and then plotted along a time series chart to determine the yearly index trends. Values outside of our determined ice, snow, and partial formation index values were removed from analysis. Each year was fitted with a spline function in R.

The team could not find pre-existing literature that defines an index threshold for river ice presence. However, Li et al. (2021) conducted research on the Tibetan plateau and supplied a basis for establishing an RDRI threshold. To determine index values for water, we analyzed the NDWI, NDII and RDRI values for an early fall image when the river was flowing water. The same methodology was applied for establishing frozen index values from winter river imagery when the rivers were frozen. Investigating threshold values present for the ice formation period was a significant and novel ambition of this feasibility study for our partner's interest in determining uncrossable periods for caribou migration.

To validate our results, we analyzed every available image without complete cloud coverage to create the annual freezing timeline chart. From observations of every available satellite image, we inspected the initial appearance of flowing ice chunks, formation of ice jams, and freezing of the river. Between days with no satellite observation, we assumed a continuation of conditions from the last image observed until there was confirmation from the next available date with an image. This established a yearly timeline of ice formation periods for each river section.

3.3.2 Radar Data Analysis
The SAR imagery was analyzed by taking the mean values for the VV and VH backscatter of the river. After taking the means of the backscatter, we plotted the time series across the 7-year study period. We then fit the plot with a spline function in R to interpolate the results by taking a moving average of the data points. We also used this time series to compare the results with the air temperature data from MesoWest. The temperature data was also plotted with the smoothing function and compared to the backscatter plots. Through ArcGIS Pro, we visualized the freezing process using VV and VH backscatter, displaying how backscatter correlates with river ice formation.

3.3.3 Optical and Radar Comparison Analysis
We created another version of the freezing timeline chart for the SAR data. We used VH and VV backscatter for each year to create thresholds for water and ice. Due to the lack of detail in the radar data, we separated the chart

into a binary decision of water versus ice presence. We then used this to compare how the optical and radar data provided details on the river freeze up timeline.

4. Results & Discussion

4.1 Analysis of Results

4.1.1 Manual Optical Analysis Results

Figure 3 shows the timing of annual freezing for each study site from 2017 to 2023. The river stages were classified into open water, flowing river ice, ice jams with partial open water, and river ice. The formation phases of flowing river ice and ice jams with open water (symbolized in red and purple) are considered high risk for caribou to cross during migration. Our analysis on river ice formation found variation in the yearly timing of the beginning of ice formation and when it has fully formed.

Our results indicate that the initial onset of ice formation varied from year to year across all three sites. East Kobuk and West Kobuk generally have similar initial flowing ice presence, with fluctuating ice jam formations and full freezing. The ice formation period for East Kobuk ranged from six to twenty-four days and full river freezing consistently occurred between October 22 and November 3. The river freezing at West Kobuk ranged between nine and seventeen days. In four out of the seven years, West Kobuk River completely froze between October 30 and November 1, with the other three occurring on earlier dates between October 14 and October 25. In 2023, there is an early appearance of flowing ice, and a lengthened formation period for both study sites.

The Colville study site typically had quicker ice formation periods than the Kobuk River with the first observed appearance of ice chunks and full freezing ranging between two to twelve days. Five out of the seven years, Colville was observed to completely freeze between October 16 and October 19. The initial presence of flowing ice chunks occurred later in 2017 – 2020 and earlier in 2021 – 2023. Overall, Colville ice formation fluctuated less than East and West Kobuk, with an earlier presence of flowing ice, and lengthening ice formation periods over the years.

The limitations of the results in Figure 3 include the gaps in image availability. Since river ice could form on days without satellite observations, capturing the exact date of river ice formation is difficult without daily observations. In 2017, East and West Kobuk had no available imagery from October 1 to October 16 due to extensive cloud coverage. While these limitations affect the exact date of river phases, Figure 3 displays the observed river ice formation periods.

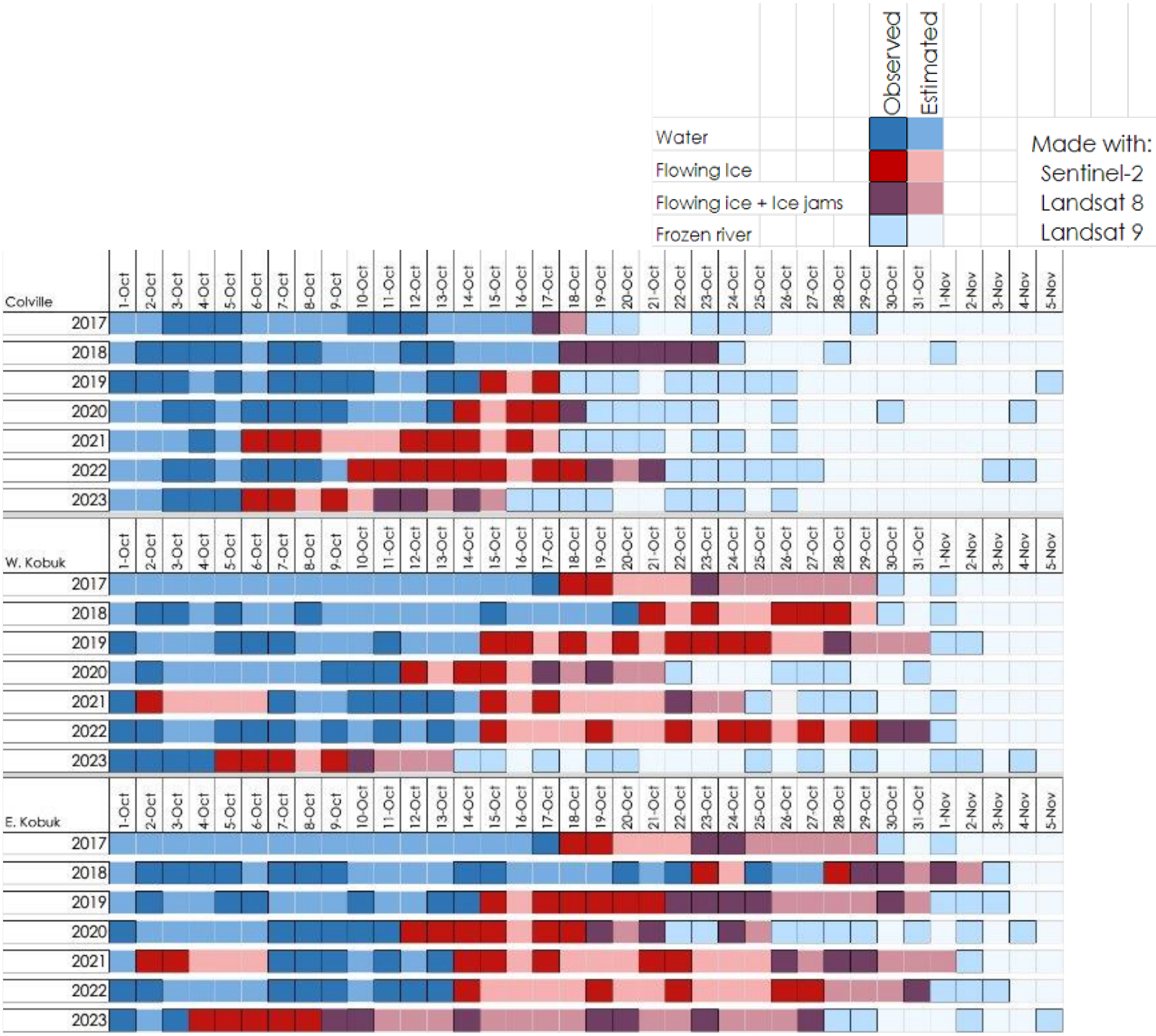

Figure 3. Timeline of yearly freezing dates for each study site from 2017 to 2023. Bolded colors indicate days with an observation, and lighter shades indicate days between observations.

4.1.2 Optical Indices Analysis Result

We quantified results from the annual freezing timeline by calculating spectral indices associated with ice detection at each study site (Figure 4; Figure 5). Existing literature characterizes NDII values close to one and zero as ice and open water, respectively. Previously, literature on RDRI and our pixel measurements on open water indicated values between 0 and 0.13 represent ice and higher values represent open water (unbounded, but generally less than 3 or 4 from our observations; Li et al., 2021). We hypothesized that each interpolated spline would contain values closer to water before ice onset, a region of shifting values during ice formation, and convergence near the corresponding ice values when the river freezes completely.

Our results somewhat support these assertions. For the RDRI index (Figure 4), the curves in each plot converge to RDRI values of 0, except for Colville in 2023. Colville had higher variability when ice completely forms, but the formation period is difficult to define when the curves do not converge in 2019 and 2020. The RDRI index detected ice later at Kobuk than Colville which is consistent with the timeline in Figure 3. Each annual curve contains a period of decreasing RDRI, but most also contain an increasing period before convergence. In Figure 4, the proceeding absolute maxima in each spline occurs at the beginning of the ice formation, indicating that high RDRI values may correspond to partially frozen ice. The subsequent ice formation period duration varies annually between approximately 10 – 20 days, raising feasibility questions about using RDRI. Furthermore, the 2019 curve in Figure 4a incorrectly suggested that ice exists in early September. While the spline shapes are somewhat consistent, RDRI values between 1 and 2 occur both before and during the ice formation period. An additional concern is interpreting index values for open water given the spatial and temporal variation across the plots.

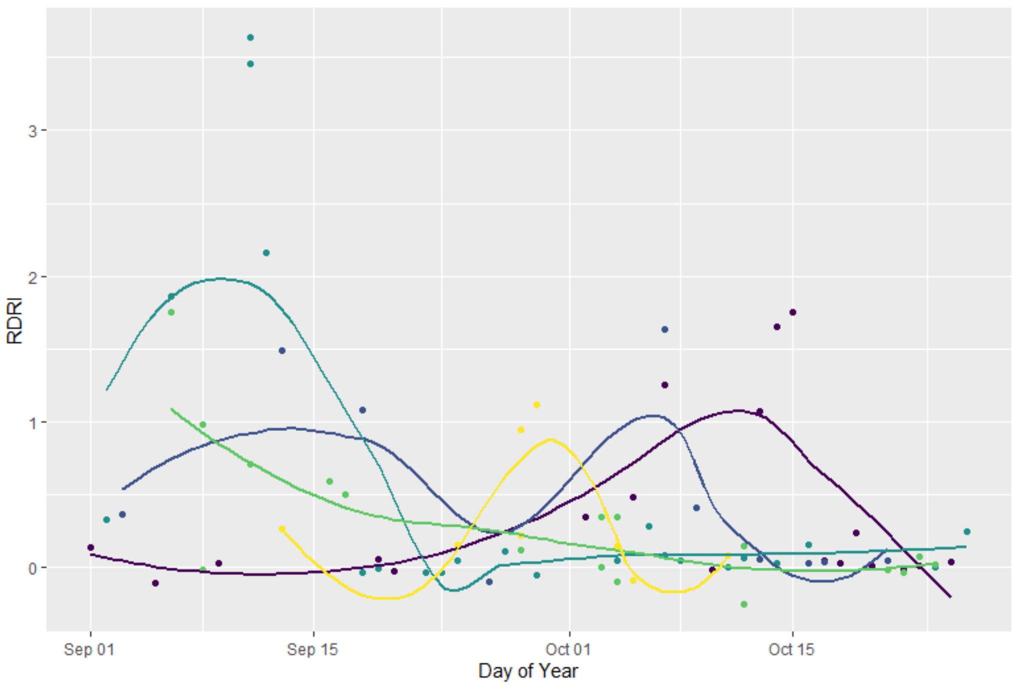

Figure 4a. Mean RDRI values by year, Colville.

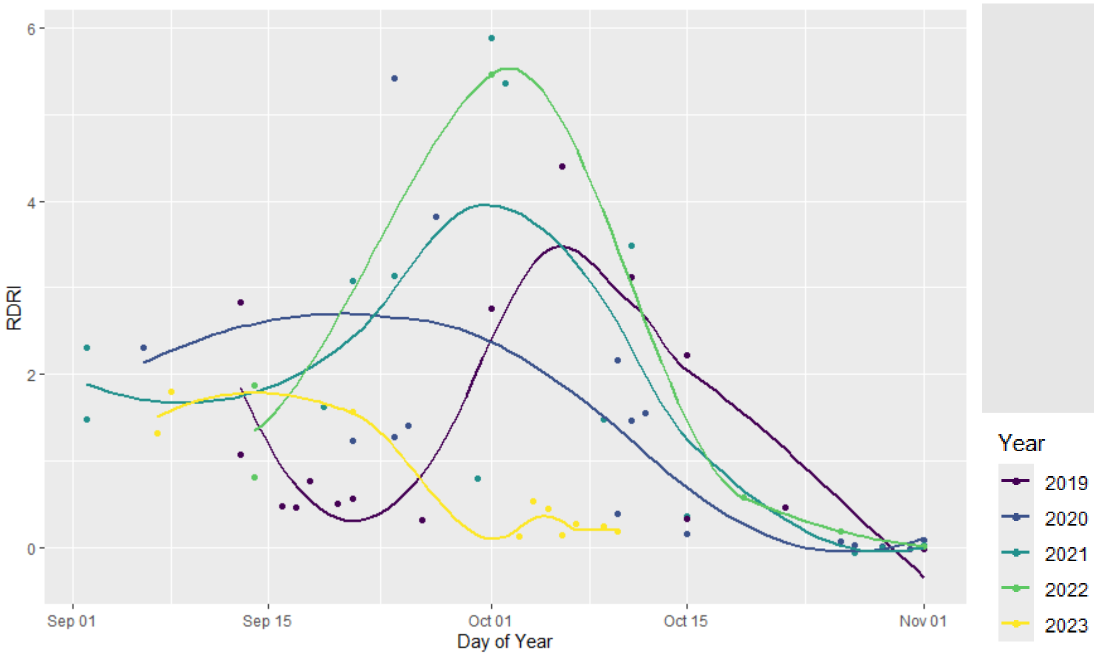

Figure 4b. Mean RDRI values by year, West Kobuk.

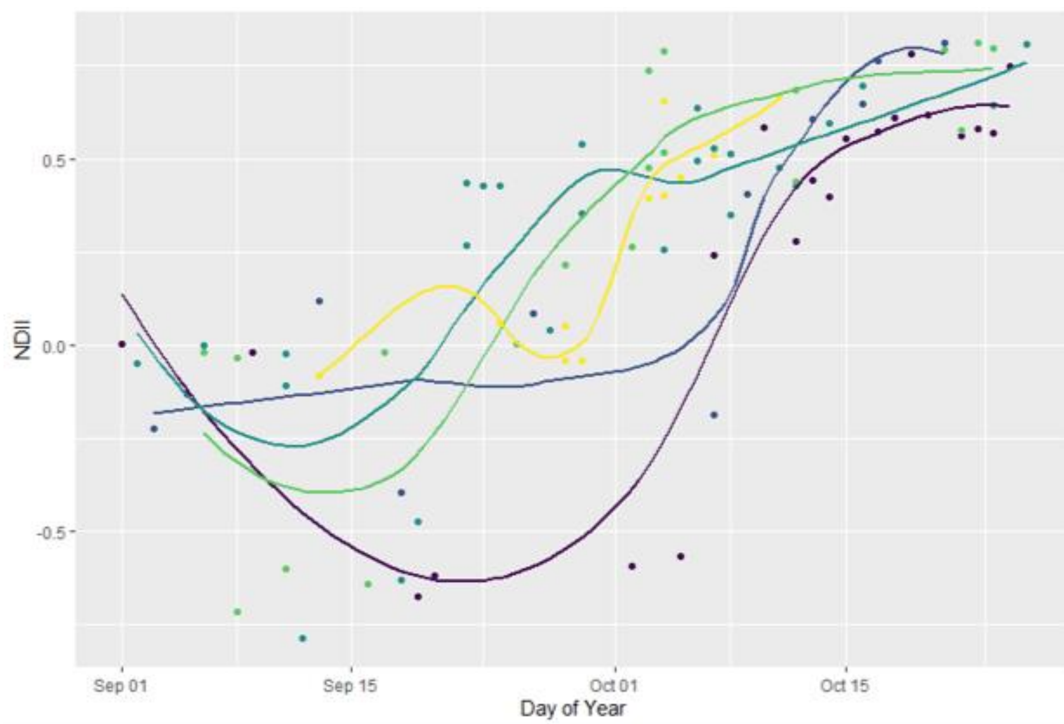

Figure 5a. Mean NDII values by year, Colville.

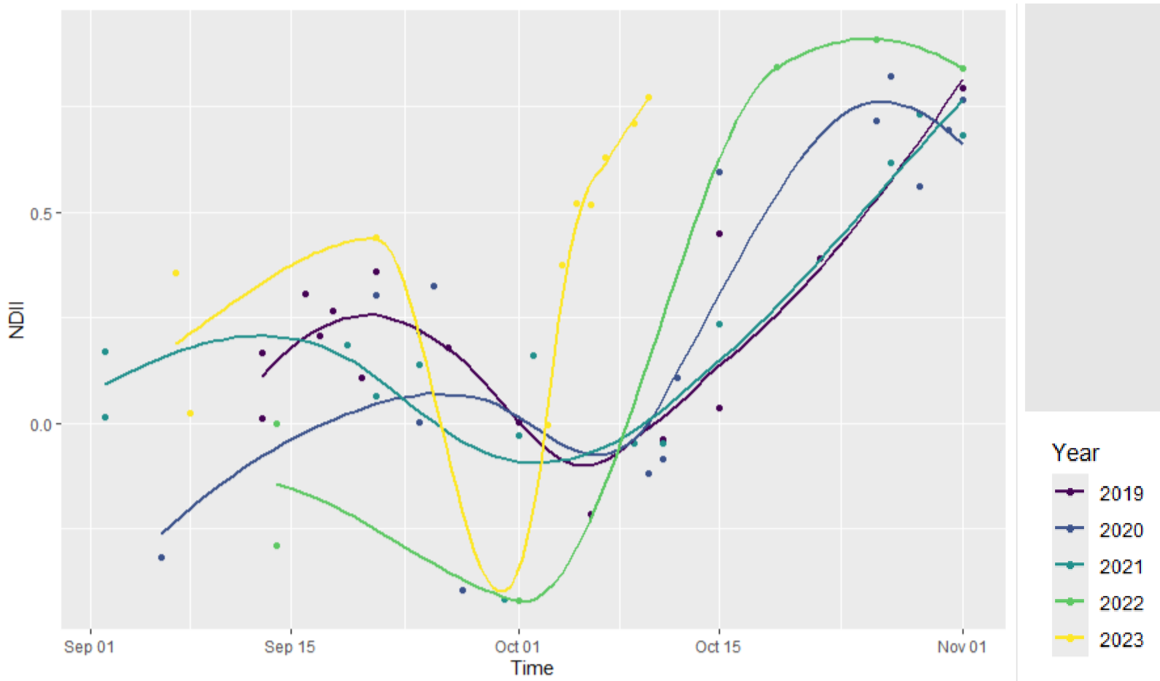

Figure 5b. Mean NDII values by year, West Kobuk.

Interpreting the NDII time series' (Figure 5) is more complex. Each plot approaches one, which is the expected ice value (NDII values are between 1 and –1), but some of the West and East Kobuk curves never stabilize or increase past expected freezing onset dates in Figure 3. According to the plots, ice onset on the Kobuk River occurs in mid to late October, which is relatively consistent with the freezing timeline dates. Inferring onset dates from the plots is further complicated by instances where the river freezes, thaws, and then refreezes, such as Kobuk in 2021. Additionally, the NDII plots assess the transition to ice less conclusively than RDRI. The 2020 and 2022 Kobuk and Colville curves illustrate these periods clearly, but the 2023 Figure 5b curve is difficult to interpret. While the NDII results are confusing, the index suggests that ice forms earlier in 2023 than in 2021 and 2022. However, we could not determine when ice becomes thick enough to support caribou crossing. We also did not observe a long-term shift in ice onset date throughout the study period.

Since the time series plot values are summarized as image means, we mapped annual NDII results to see how the values are dispersed over the rivers. These visualizations depict annual changes in ice extent to determine when various river locations transition from water to partial ice to fully formed ice. Figure 6 illustrates the results for an eleven kilometer stretch on the Colville River in 2019. While there is snow on October 7, the contiguity of the dark blue region throughout the image indicates that the river is entirely open water. The October 17 image, selected because it occurs during the 2019 formation period (Figure 6), shows substantially more frozen cover along the river than on October 7. The open water zone is consistently narrower and no longer present in the image center. The river is narrowest at the end of October, and the upper left and lower right river regions froze over entirely. Mapping NDII highlights similar advantages and challenges of applying spectral indices to ice detection. The October 17 image illustrates the partially frozen period shown in Figure 6b and may be useful in determining where caribou can cross. However, it is unlikely that the Colville River contained open water on October 25 based on the optical imagery true color composites.

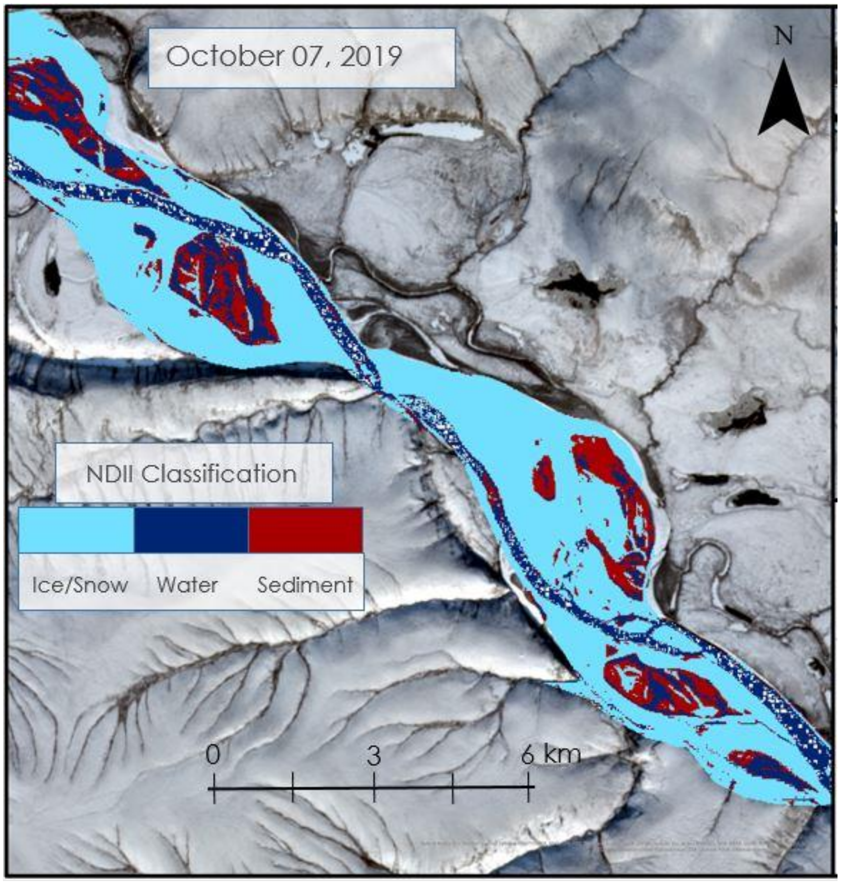

[Basemap Credit: State of Alaska, Esri, TomTom, Garmin, StateGraph, METI/NASA, USGS, EPA, NPS, USDA, USFS, Esri, USGS]

Figure 6a. Fall 2019 Time Series Ice Formation Map in Colville River: Oct 7, 2019.

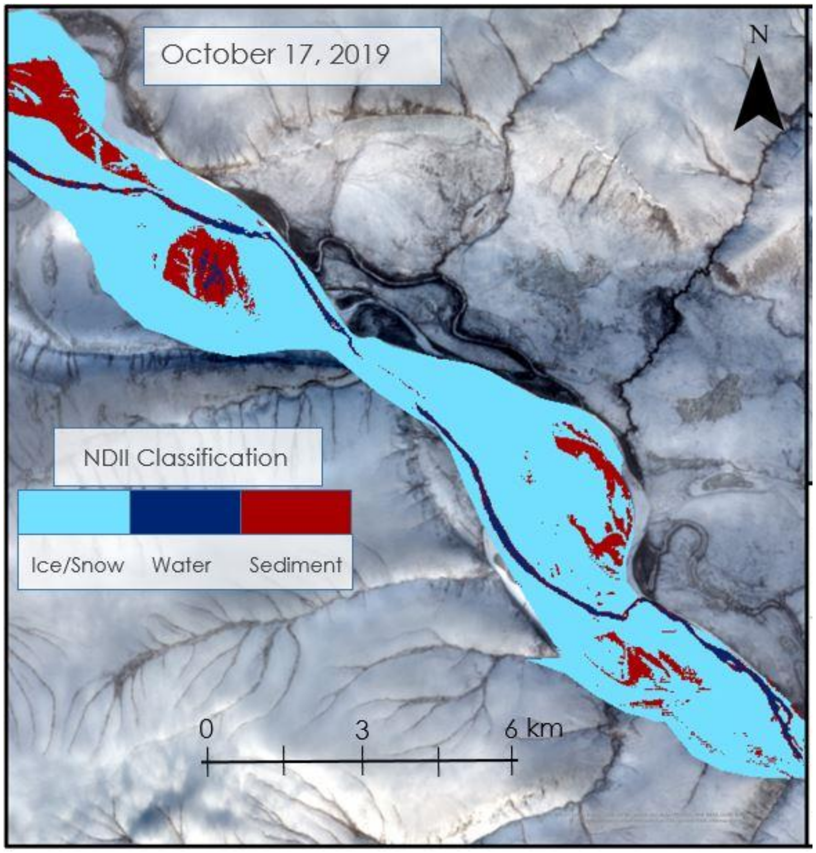

[Basemap Credit: State of Alaska, Esri, TomTom, Garmin, StateGraph, METI/NASA, USGS, EPA, NPS, USDA, USFS, Esri, USGS]

Figure 6b. Fall 2019 Time Series Ice Formation Map in Colville River: Oct 17, 2019.

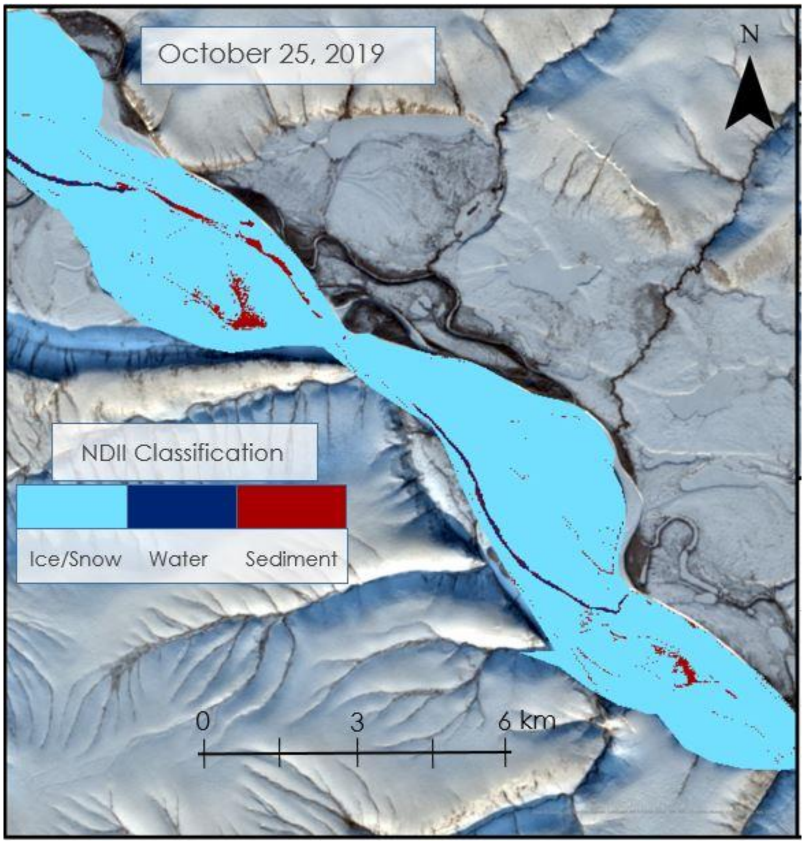

[Basemap Credit: State of Alaska, Esri, TomTom, Garmin, StateGraph, METI/NASA, USGS, EPA, NPS, USDA, USFS, Esri, USGS]

Figure 6c. Fall 2019 Time Series Ice Formation Map in Colville River: Oct 25, 2019 (c).

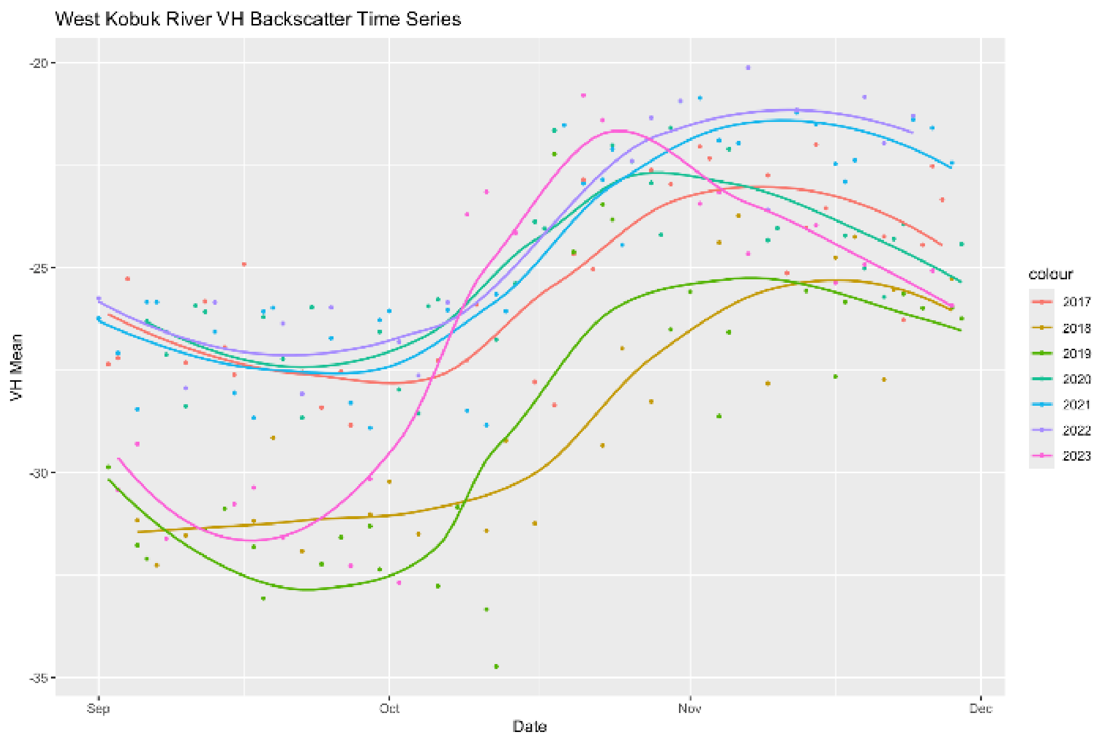

Figure 7a. VH backscatter mean by year, West Kobuk.

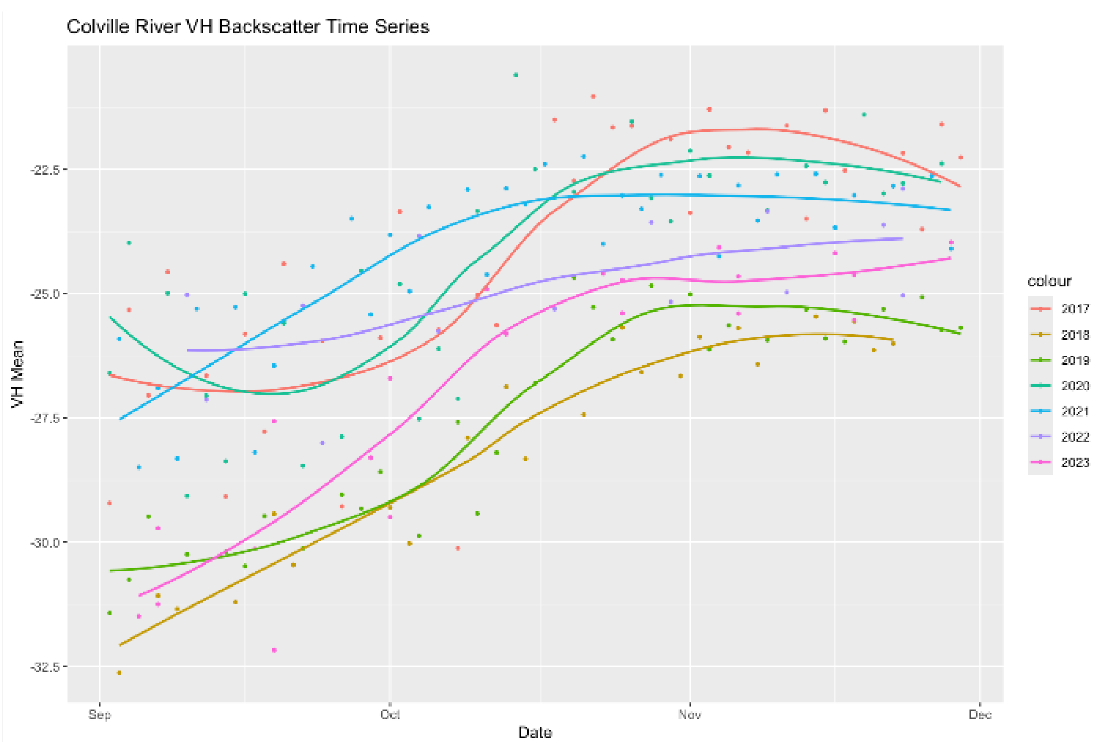

Figure 7b. VH backscatter mean by year, Colville.

4.1.3 SAR Analysis Results

SAR backscatter is low when the surface is smooth (e.g., open water), as there is less radar signal backscattering, and they are high when the surface is rougher with more signal scatter. The results from the Sentinel-1 imagery showed that the VH and VV mean backscatter was consistently low in September when water was present and relatively higher in November after the ice was formed. This is reinforced by the study done by Stonevicius et al. (2022), who saw that water has very low backscatter and land and ice typically have relatively high backscatter. According to Figure 7, the VH backscatter values increased linearly during the fall ice formation period annually across most study sites. However, the inflection points along the x-axis shift at two dates annually; first when the ice formation begins and again when the ice is fully formed. For example, in 2023 the ice formation began a little after mid-September (Figure 7a), which is around two weeks earlier than most years. The slope during migration is a lot steeper in 2023, showing that the ice formed quicker this year and in 2019, ice began forming in mid-October. The Colville River (Figure 7b) follows a different pattern than the Kobuk River, which is expected because of its higher latitude and the plot suggests that ice formation is happening earlier at Colville. The linear portion of most of the plots are steeper than the other study sites indicating a quicker formation period. The spline functions shown in 2021 and 2022 vary from other years indicating a different pattern in ice formation in Figure 7b. The 2021 plot suggests water is not present for very long and the river jumps to ice cover quickly.

It is unclear why there is a yearly variation in backscatter values. Based on Figure 7, in 2018, 2019, and 2023 when water is present, VH values are lower in September than other years, and this continues over the season. We do not know why this is the case, leading to a limitation of SAR, that it is difficult to assign an exact classification to the VH backscatter values on their own or across years. Instead, water and ice thresholds are made by looking at the overall trend of the radar signal in an isolated setting (e.g., over a single freezing season). In the case of this study, water, partial ice, and ice backscatter thresholds were made on a year-by-year basis. A similar trend is seen for VV backscatter (Figure C2).

The correlation between air temperature and VH backscatter means over the western stretch of the Kobuk River was analyzed to help fill in satellite data gaps. The temperature data was taken from the Kiana weather station on the Western part of the Kobuk River. Before the average air temperature reaches 0°C, the VH backscatter values begin to increase as ice begins to form (Figure 8). At the point when air temperature is 0°C, around mid-October, the backscatter is at similar points of the smooth function for each year, marked by the vertical blue line. As the temperature lowers, the backscatter continues to increase while ice forms.

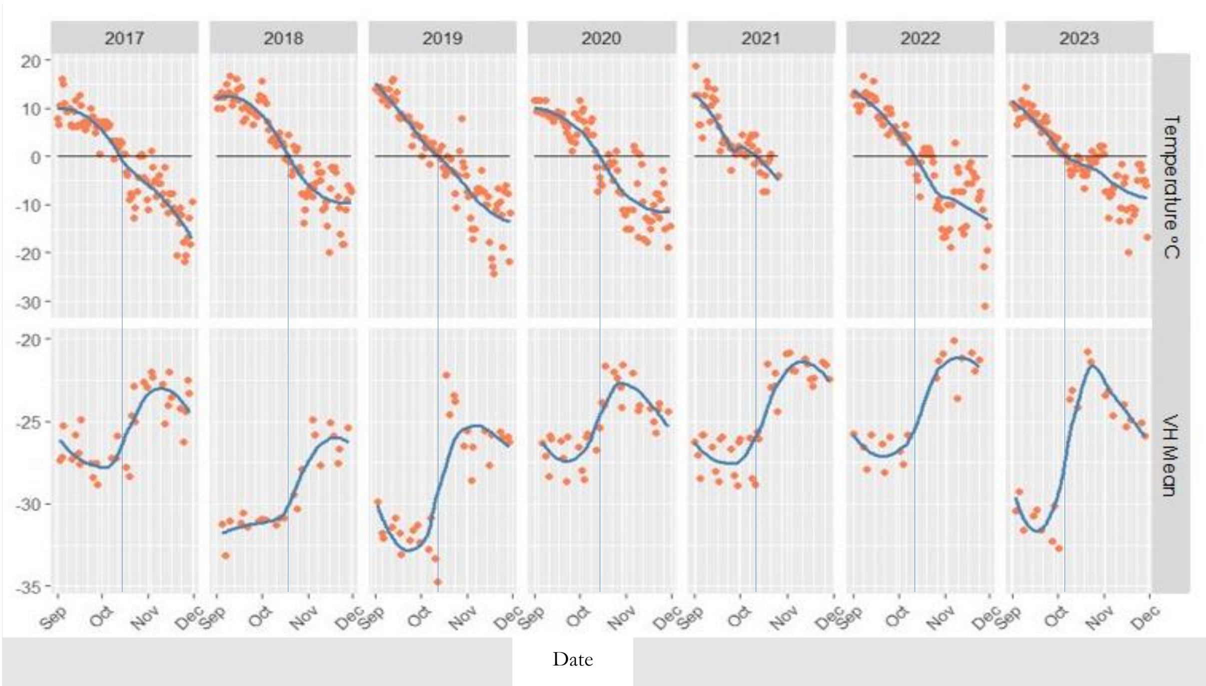

Figure 8. Temperature over VH backscatter mean, West Kobuk.

In addition to plotting the backscatter time series, we also mapped the VV and VH backscatter for the fall of 2020. We created these maps to show the dispersion of VV backscatter values along the West Kobuk River on different days in the fall (Figure 9; Figure D1; Figure D3). The images follow the same trend as what was seen in the backscatter time series plots where backscatter is lower in early fall and by the end of October, it is high. The darker blue area of the river indicates a smoother surface, which can be seen as water while the lighter blue is reflective of rougher surfaces, possibly depicting ice. According to Brown et al. (2023), smooth ice may result in lower values of backscatter as there is less radar signal scatter. We predict that the royal blue areas in Figure 9c are areas of the river with smooth ice as the values came out a little lower even though the river is frozen (Brown et al., 2023).

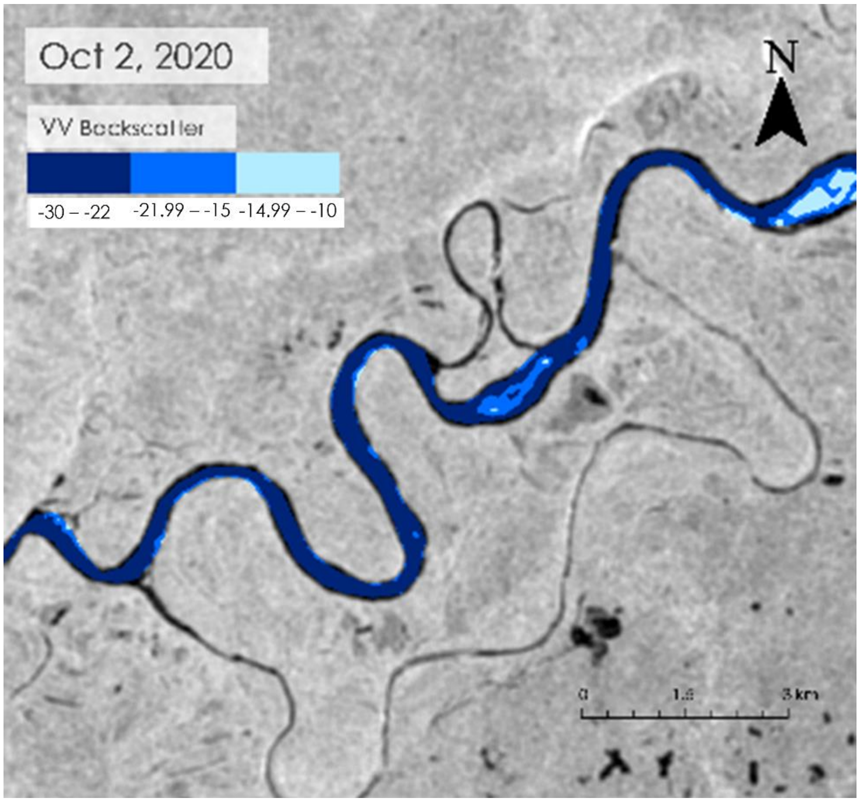

Figure 9a. Fall 2020 Freezing timeline in a section of the West Kobuk River using VV, Oct 2, 2020.

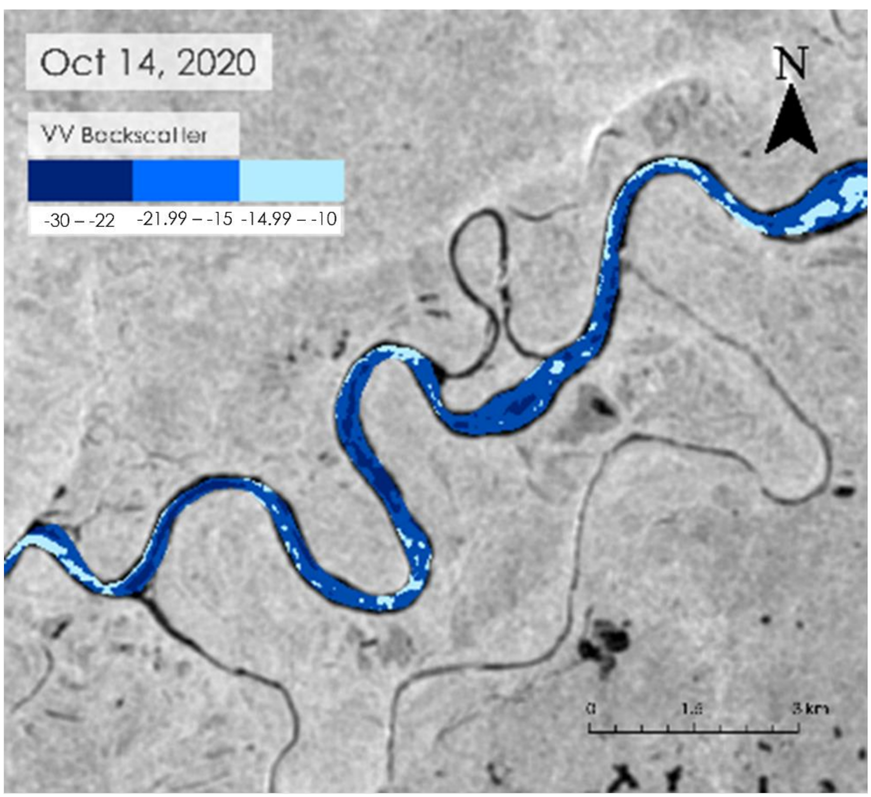

Figure 9b. Fall 2020 Freezing timeline in a section of the West Kobuk River using VV, Oct 14, 2020 (b).

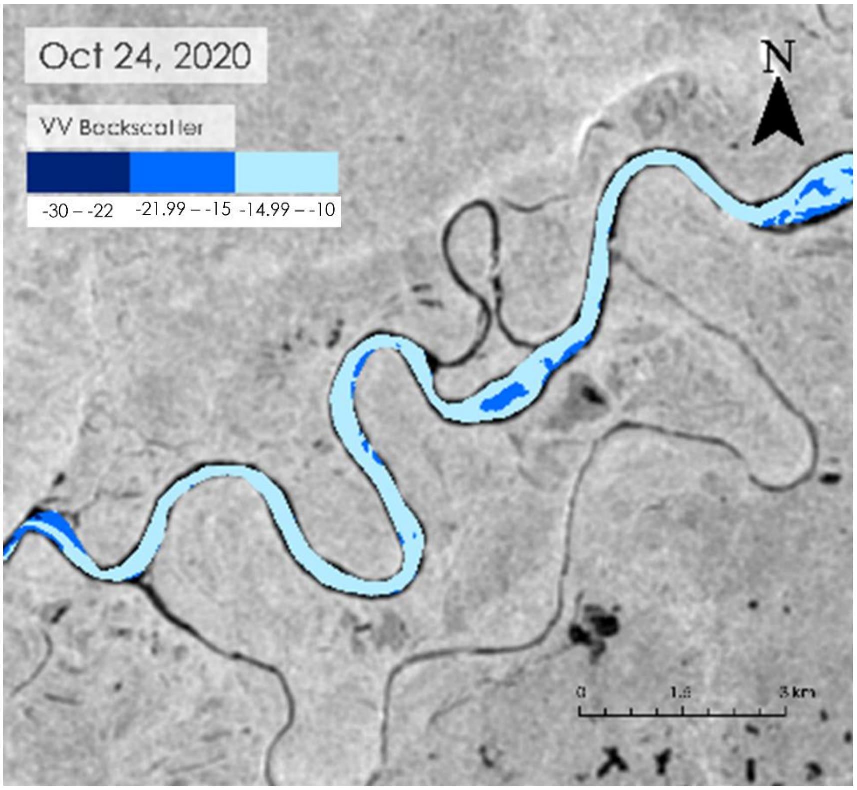

Figure 9c. Fall 2020 Freezing timeline in a section of the West Kobuk River using VV, Oct 24, 2020.

We replicated the analysis for one day on each year in mid-October from 2017 to 2023. The dates were selected to be as close to one another as possible during the river ice formation time. However, because of satellite imagery availability this was not always possible as Sentinel-1B was discontinued in 2022. In 2017, the VV mean values were low indicating a smooth surface of water. 2019 had a high VV value meaning the river's surface became rougher indicating ice had already formed by October 18, 2019. Similar to the smooth ice that was seen in Figure 9 and Figure D2, we predict that the royal blue parts of Figure 10c are areas of smooth, fully formed ice.

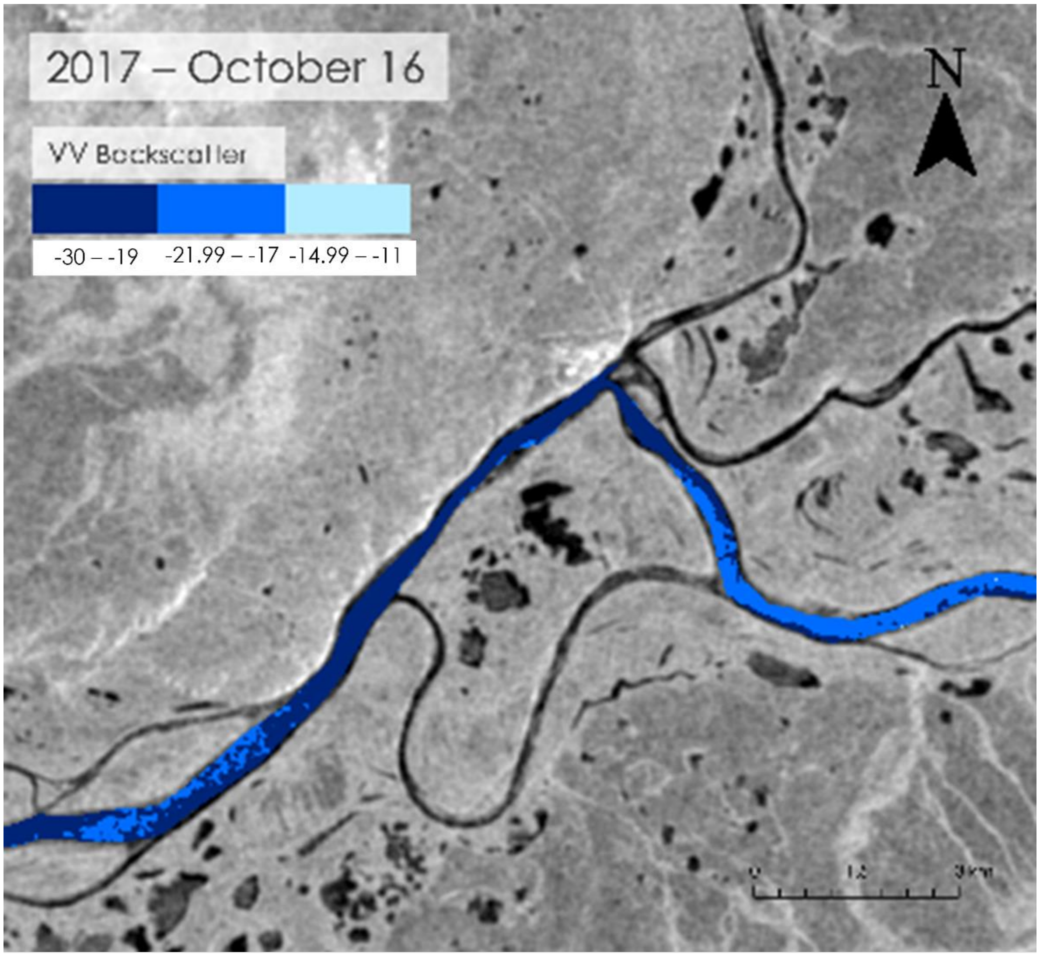

Figure 10a. Mid-October over the years in a section of the West Kobuk River using VV, Oct 16, 2017.

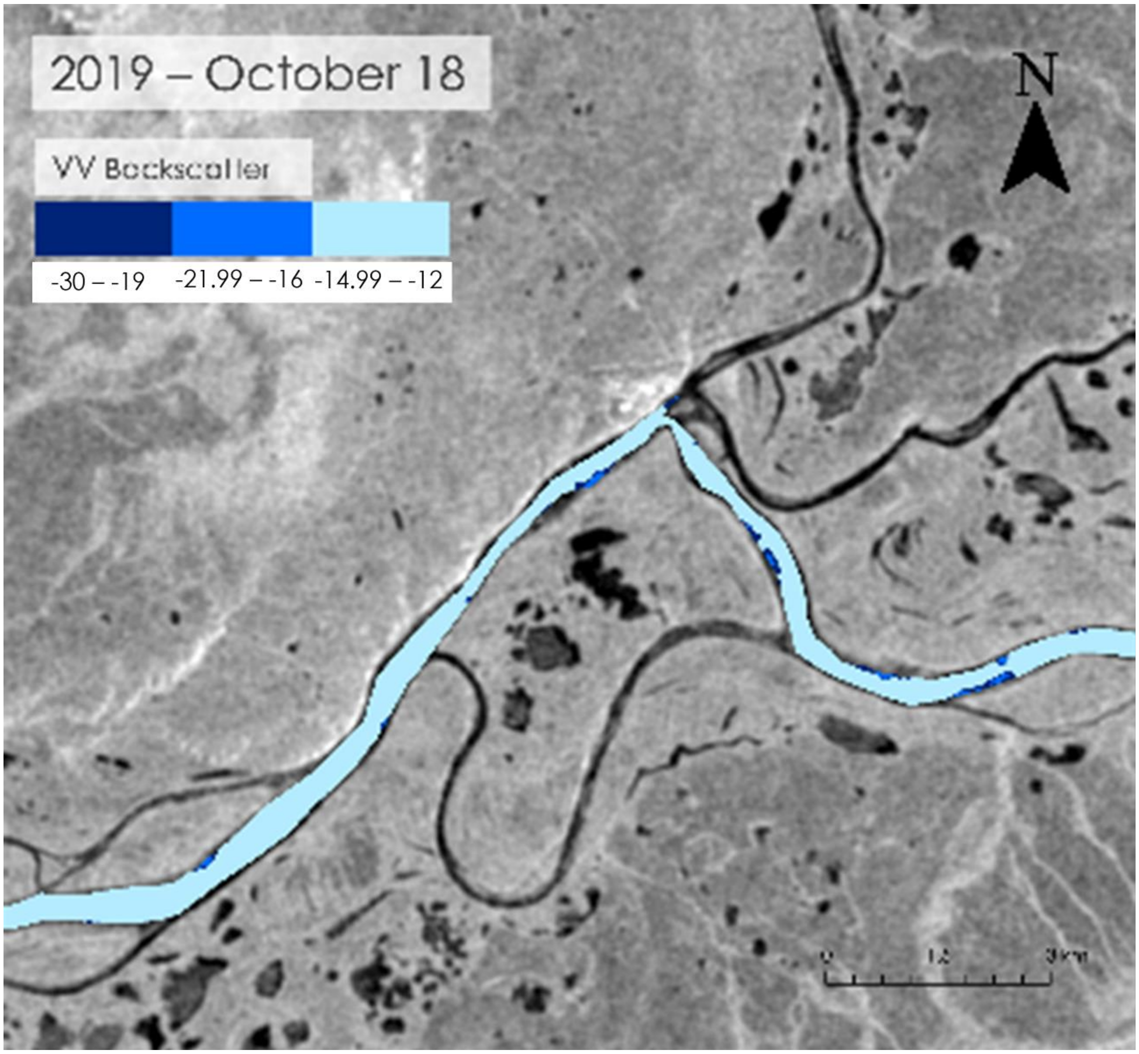

Figure 10b. Mid-October over the years in a section of the West Kobuk River using VV, Oct 18, 2019.

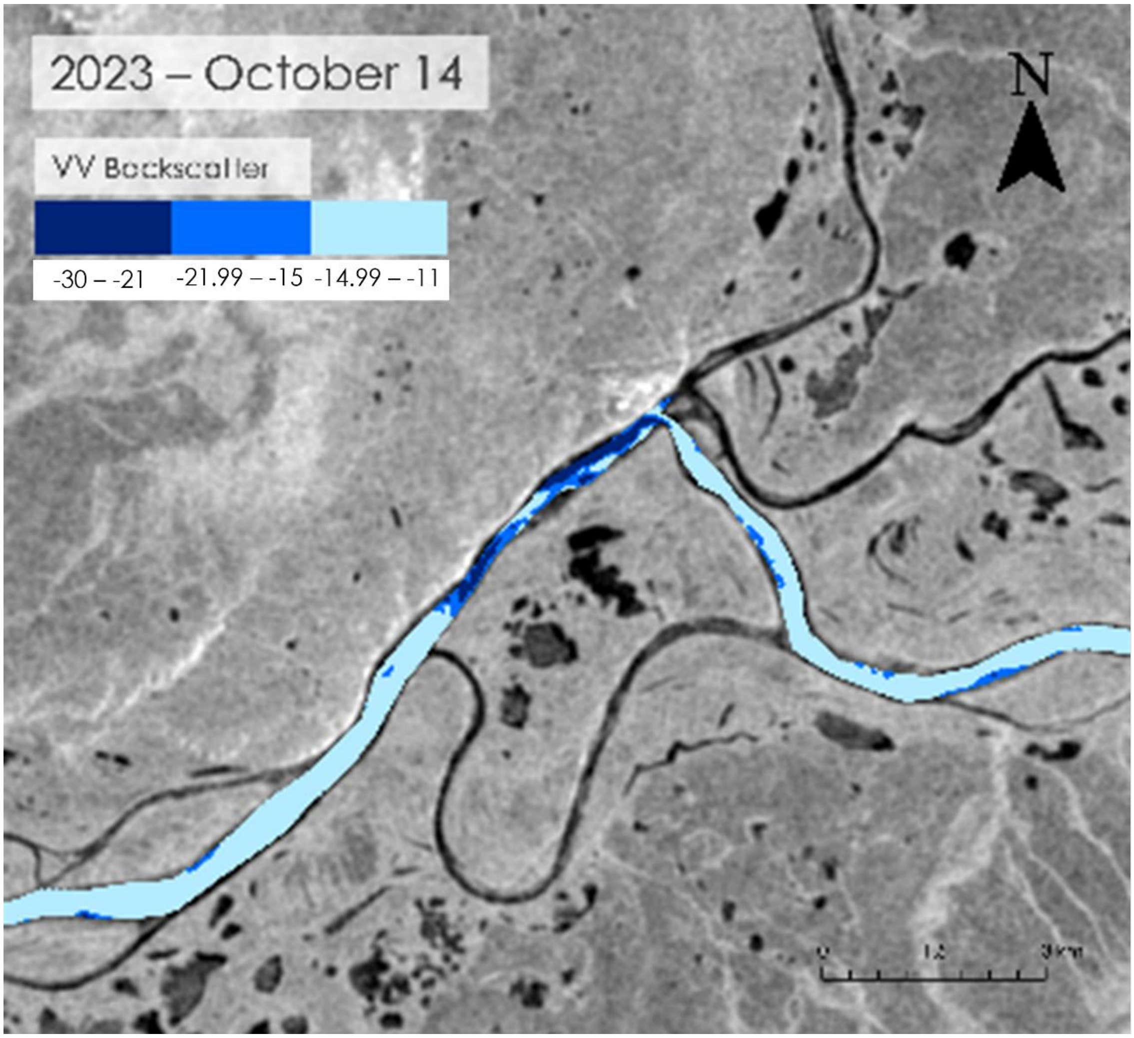

Figure 10c. Mid-October over the years in a section of the West Kobuk River using VV, Oct 14, 2023.

4.1.4 Comparative SAR with Optical Analysis Results

To test the SAR and optical data's consistency, we ran statistics on the binary chart showing water versus ice presence for each sensor type (Figure E1). We found that during ice formation, both datasets had 179 images in total which overlapped 64 times. This created 32 instances where both types of sensors had data on the same day to compare. Out of the 32 instances, the images contradicted 9.37% of the time and were affirmed 90.62% of the time. There are only three days where the results are contradictory as shown on the chart (Figure 3). For example, on Oct 12, 2021, the SAR data detected ice cover while optical data detected water. However, based on observations a day before and after, on Oct 11, 2021, and Oct 13, 2021, SAR data recognized water presence, thus we can assume that the SAR result on Oct 12, 2021, was an outlier due to misinterpretation or wind interference.

4.2 Feasibility for Partner Use

While optical data showed promise in being able to cross-validate radar analysis, Landsat 8, Landsat 9, and Sentinel-2 had lower temporal resolution compared to Sentinel-1 but higher image availability when used together. As the Sentinel-2 constellation produces an image every fifth day, and Landsat 8 & 9 together will produce an image every eighth day. Meanwhile the Sentinel-1 constellation images every sixth day until 2022.

However, optical sensors have far less image availability and more inconsistency when sorting for images with low cloud coverage, whereas SAR data is not limited by clouds. While SAR is not affected by clouds, the limitations lie in interpreting the backscatter data and the possibility of wind interference increasing the values (Stonevicius et al., 2022). Although Sentinel-2 had available imagery later in the year than the Landsat series, which was limited farther into the fall, Sentinel-2 had no atmospherically corrected data in North America for the years 2017 and 2018. This shortage of atmospherically corrected data was supplemented by using Sentinel-2 level 1 imagery for 2017 & 2018 in the yearly freezing dates analysis. Although we expected the Harmonized Landsat Sentinel dataset to provide higher temporal resolution for optical data and irregularities in seasonal extent provided less viable imagery than using the Landsat series and Sentinal-2 independently (Claverie et al., 2018). Overall, we found that SAR backscatter is the most suitable method for detecting trends in river ice, while optical data was the most suitable for detecting the onset of ice.

4.3 Future Recommendations

To help improve the results derived from optical imagery, future research should use satellite imagery with a higher temporal resolution. Since there was no atmospherically corrected Sentinel-2 in GEE, our study contained considerable data gaps. Aggregating optical imagery from additional software would increase confidence in our results, providing a more holistic assessment of Alaskan river ice phenology. This includes using the Harmonized Landsat Sentinel dataset and the recently launched Landsat 9 OLI-2. Given the uncertainties from our time series plot, it is necessary to apply more comprehensive data validation techniques. Validating with multiple locations can better account for spatial heterogeneity in air and water temperature throughout each river. We recommend supplementing these measurements using in situ ice observations, providing ice cover type and thickness information that contemporary remote sensing methods cannot reliably detect. This can help define thresholds for crossable ice to conduct better caribou migration risk assessments at river crossing areas. Another way to validate the yearly ice onset dates is to use the caribou tracking GPS data which was a collaborative effort between NPS, Alaska Department of Fish and Game, Yukon Environment, US Geological Survey, and the US Fish and Wildlife Service (Cameron et al., 2021). We did not have access to the protected data for this project to compare with our results, but future analysis can strengthen the findings. Furthermore, the caribou tracking data can be compared with our observations to investigate when caribou crossed over the river to wintering grounds in the fall. Finally, optical and radar imagery limitations underscore the importance of developing more advanced ice detection workflows. Future researchers should develop a supervised classification model to better detect ice and quantify its strength. This algorithm should be trained on images of varying time, atmospheric condition, and topography to better inform the decision making of our project partners.

Future work studying how different phenology patterns impact the Western Arctic Herd will be pursued in a second part of this project, which will be conducted during Summer 2024. After seasonal migrations, caribou aim to calve in areas with healthy, abundant vegetation that provides nourishment for their calves. Using Earth observations, this project will detect changes in vegetation phenology through time series analysis to see if caribou migrations target the time and areas of peak vegetation. As the conclusion to this project, this, in conjunction with results on river ice phenology, will help to understand how changes in ecological trends have shifted caribou migration behavior.

5. Conclusions

This project uses remote sensing techniques to help the National Park Service detect river ice cover throughout the Colville and Kobuk rivers. We analyzed ice onset dates and fall formation periods between 2017 and 2023 to generate annual timelines and time series plots and maps. While we hypothesized that recent climate changes may have altered river ice phenology, the results did not illustrate any significant annual patterns in river ice formation, likely due to the study period being too short to confidently conclude annual trends. However, we detected various discrepancies during individual years. For example, ice formed the earliest in 2023 across all sites, and a brief freeze period occurred at Kobuk in early 2021 before winter-length freezing. We also observed latitudinal variation between river freezing intervals, as Colville froze earlier and quicker than Kobuk.

One project objective was evaluating the feasibility of using different sensor types in river ice applications. Quantitative analysis of radar data was more accurate in detecting ice than analysis of optical indices. According to the time series plots (Figure 4; Figure 5; Figure 7), backscatter correlates river ice better than the optical spectral indices we calculated. The radar time series spline functions are shaped relatively consistently across years and river locations, due to the surface properties of ice and open water. The RDRI and NDII curves contain similarities but are difficult to interpret without the freezing timeline or time series map. Index errors may result from spectral similarities between ice and sediment, as well as spectral interference from surrounding snow cover. The usefulness of RDRI and NDII in ice detection is largely unstudied and merits additional research. While backscatter and ice are more correlated, we found no clear decision threshold for separating ice and water. Inspecting optical true color composites thus better identifies annual ice onset dates, although radar is useful for filling data gaps.

The yearly freezing timeline created through manual optical analysis (Figure 3), provided reasonable results of formation periods through a researcher directly observing river characteristics of each image. By using multiple satellites, it was possible to increase temporal resolution, however, results were limited by cloud cover interference. Incorporating an NDWI index can aid in the manual analysis by distinguishing between open water or black ice which can appear similar in true color analysis. While this was not an automated process, by inspecting each image for river characteristics, we found that the results displayed river ice formation periods effectively for our research partners objectives.

Our results can help the National Park Service better assess the impacts of river ice phenology on terrestrial migration patterns. The yearly timelines and time series plots will help them determine when caribou can cross rivers safely in the fall and how those dates change over time. The time series maps provide further information, helping the National Park Service identify specific frozen regions throughout each river. While these visualizations are site specific, our methodology is replicable for any year and river location, provided images are available. The National Park Service can analyze migration patterns with river ice formation to contextualize recent caribou population trends and implement these monitoring strategies for caribou, which are a critical species to the broader ecosystem structure and local populations.

6. Acknowledgements

The Alaska Ecological Conservation team would like to thank our project partner Dr. Kyle Joly from the National Park Service guidance on this project. We are grateful to our science advisor Dr. Cédric Fichot at Boston University for his support and guidance throughout the project's duration. We would also like to thank our node lead Madison Arndt at the Boston NASA DEVELOP office, and special thanks to Seamore Zhu at Boston University for technical support.

This material contains modified Copernicus Sentinel data (2017 – 2023), processed by ESA.

Any opinions, findings, and conclusions or recommendations expressed in this material are those of the author(s) and do not necessarily reflect the views of the National Aeronautics and Space Administration.

This material is based upon work supported by NASA through contract 80LARC23FA024.

7. Glossary

Backscatter – the portion of the outgoing radar signal that the target redirects directly back towards the radar antenna; used in Sentinel-1 SAR. It is a measure of reflective strength of the radar target
Index – A spectral index is a mathematical combination of two or more wavelengths that enhances the information content of the data (Rouse et al., 1974)
NDII – Normalized Difference Infrared Index
NDWI – Normalized Difference Water Index
Optical Imagery – Satellite Imagery captured on the visible spectrum, near-infrared, and short-wave infrared bands (wavelengths)
Phenology – the study of cyclic and seasonal natural phenomena

RDRI – Relative Difference Ice Index
SAR (C-Band) – Synthetic Aperture Radar
VH (Mean) – Cross-polarized radar signal, transmits vertical waves and receives horizontal; mean represents a mean of pixel value over a selected area.
VV (Mean) – Co-polarized radar signal, transmits vertical waves and receives vertical; mean represents a mean of pixel value over a selected area.

8. References

Brown, D. R. N., Arp, C. D., Brinkman, T. J., Cellarius, B. A., Engram, M., Miller, M. E., & Spellman, K. V. (2023). Long-term change and geospatial patterns of river ice cover and navigability in Southcentral Alaska detected with remote sensing. *Arctic, Antarctic, and Alpine Research, 55*(1), 2241279. https://doi.org/10.1080/15230430.2023.2241279

Cameron, M.D., Eisaguirre, J.M., Breed, G.A. *et al.* (2021) Mechanistic movement models identify continuously updated autumn migration cues in Arctic caribou. *Mov Ecol* **9**, 54 (2021). https://doi.org/10.1186/s40462-021-00288-0

Cameron, M.D., K. Joly, and J. Hepler. (2021). New insights from an enduring tool: Using GPS data to detect calving events in Alaskan caribou herds. *Alaska Park Science, 20*(1): 84-87.

Claverie, M., Ju, J., Masek, J. G., Dungan, J. L., Vermote, E. F., Roger, J.-C., Skakun, S. V., & Justice, C. (2018). The Harmonized Landsat and Sentinel-2 surface reflectance data set. *Remote Sensing of Environment, 219,* 145–161. https://doi.org/10.1016/j.rse.2018.09.002

Earth Engine Data Catalog (2024). *Sentinel-2 MSI: MultiSpectral Instrument, Level-2A | Earth Engine Data Catalog*. Google for Developers. https://developers.google.com/earth-engine/datasets/catalog/COPERNICUS_S2_SR

Fullman, T.J., Joly, K. & Ackerman, A. (2017). Effects of environmental features and sport hunting on caribou migration in northwestern Alaska. *Mov Ecol* **5**, 4. https://doi.org/10.1186/s40462-017-0095-z

Gao, B. (1996). NDWI—A normalized difference water index for remote sensing of vegetation liquid water from space. *Remote Sensing of Environment, 58*(3), 257–266. https://doi.org/10.1016/S0034-4257(96)00067-3

Ji, L., Zhang, L., Wylie, B. K., & Rover, J. (2011). On the terminology of the spectral vegetation index (NIR − swir)/(nir + SWIR). *International Journal of Remote Sensing*, *32*(21), 6901–6909. https://doi.org/10.1080/01431161.2010.510811

Joly, K., Gunn, A., Côté, S. D., Panzacchi, M., Adamczewski, J., Suitor, M. J., & Gurarie, E. (2021). Caribou and reindeer migrations in the changing Arctic. *Animal Migration*, *8*(1), 156–167. https://doi.org/10.1515/ami-2020-0110

Le Corre, M., Dussault, C., & Côté, S. D. (2017). Weather conditions and variation in timing of spring and fall migrations of migratory caribou. *Journal of Mammalogy*, *98*(1), 260–271. https://doi.org/10.1093/jmammal/gyw177

Leblond, M., St-Laurent, M.-H., & Côté, S. D. (2016). Caribou, water, and ice – fine-scale movements of a migratory arctic ungulate in the context of climate change. *Movement Ecology*, *4*(1), 14. https://doi.org/10.1186/s40462-016-0079-4

Li, H., Li, H., Wang, J., & Hao, X. (2021). Identifying river ice on the Tibetan Plateau based on the relative difference in spectral bands. *Journal of Hydrology*, *601*, 126613. https://doi.org/10.1016/j.jhydrol.2021.126613

MesoWest (2024). *Surface Map / Alaska Fire & Fuels* [Data set]. MesoWest. https://akff.mesowest.org/map/#/c6337,-14900,4/g1/mc/vtemp/sAK/n/zt

Mowat, G., Heard, D. C., & Curtis, P. J. (2023). Combining stable isotope ratios with elemental concentrations to improve the estimation of terrestrial carnivore diets. *Global Ecology and Conservation*, *45*, e02507. https://doi.org/10.1016/j.gecco.2023.e02507

Nicholson, K. L., Arthur, S. M., Horne, J. S., Garton, E. O., & Vecchio, P. A. D. (2016). Modeling Caribou Movements: Seasonal Ranges and Migration Routes of the Central Arctic Herd. *PLOS ONE*, *11*(4), e0150333. https://doi.org/10.1371/journal.pone.0150333

Rouse, J.W., Haas, R.H., Schell, J.A. and Deering, D.W. (1974) Monitoring Vegetation Systems in the Great Plains with Erts. Nasa Special Publication, 351, 309.

Stonevicius, E., Uselis, G., & Grendaite, D. (2022). Ice Detection with Sentinel-1 SAR Backscatter Threshold in Long Sections of Temperate Climate Rivers. *Remote Sensing, 14*(7). https://doi.org/10.3390/rs14071627

U.S. Geological Survey (2024). *Landsat Collection 2 Surface Reflectance* [Data set]. USGS. https://www.usgs.gov/landsat-missions/landsat-collection-2-surface-reflectance

U.S. Geological Survey (2022). *National Hydrography Dataset* [Data set]. USGS. https://www.usgs.gov/national-hydrography/national-hydrography-dataset?qt-science_support_page_related_con=0#qt-science_support_page_related_con

9. Appendices

Appendix A

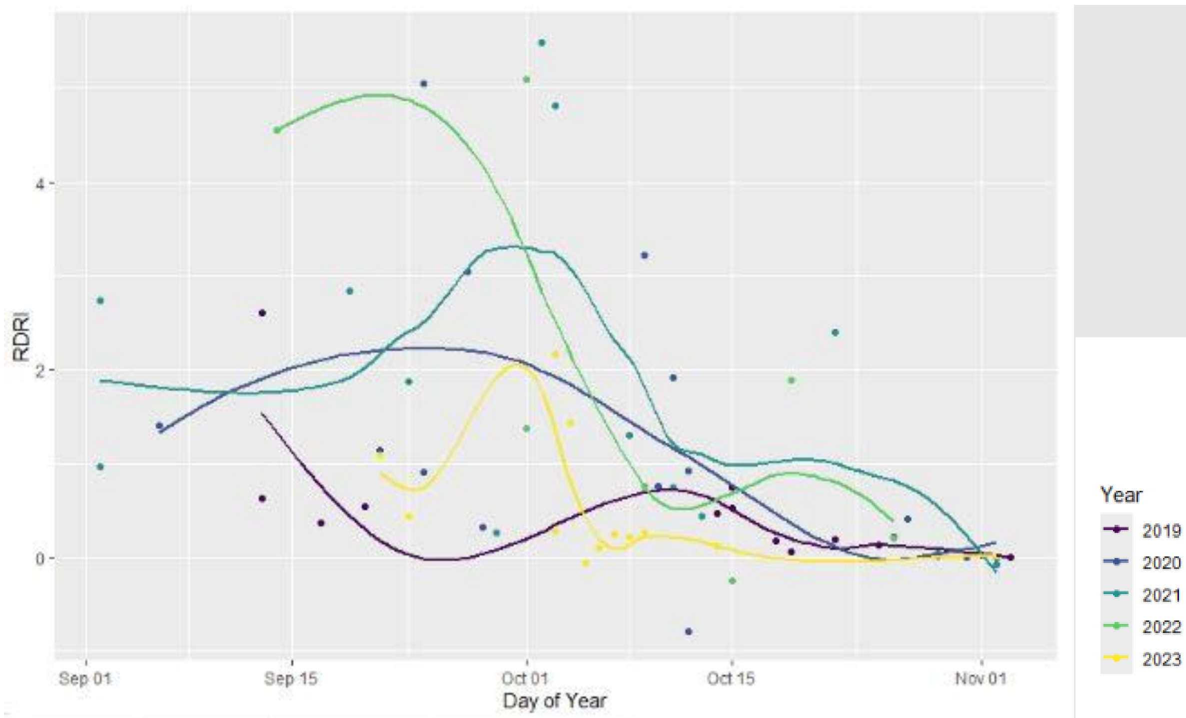

Figure A1. Mean RDRI values by year in East Kobuk.

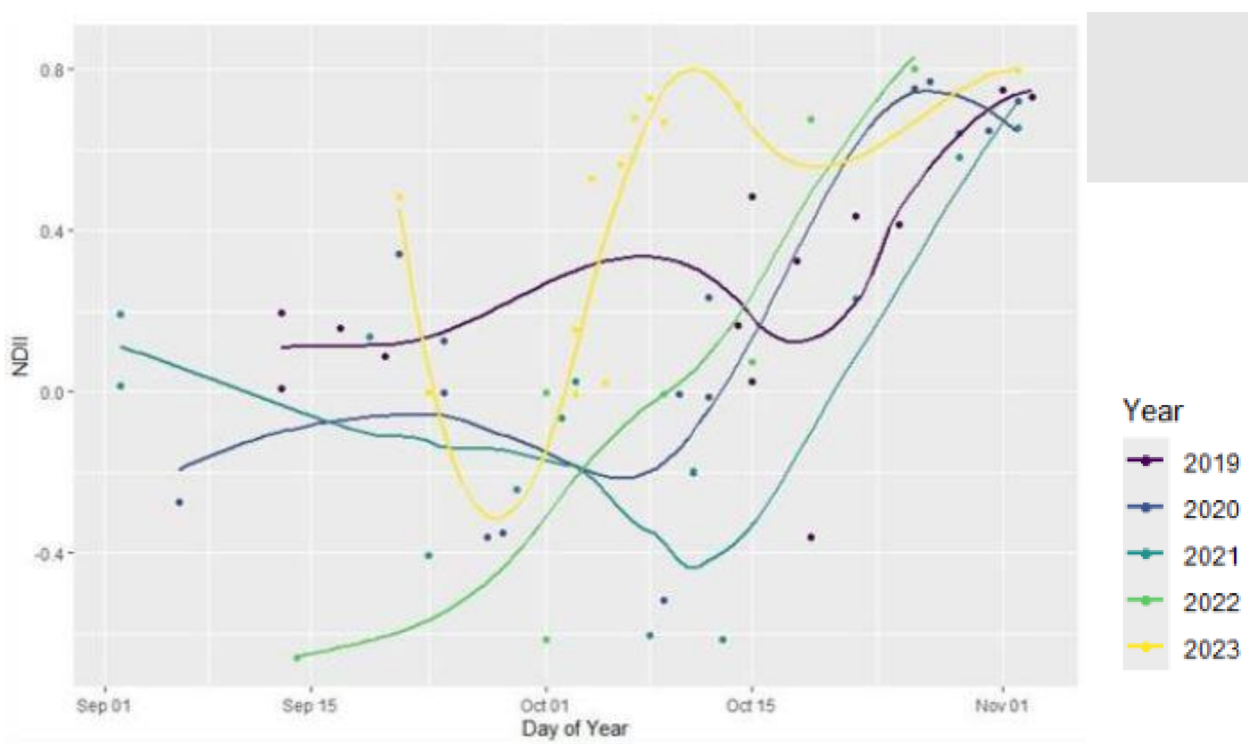

Figure A2. Mean NDII values by year in East Kobuk.

Appendix B

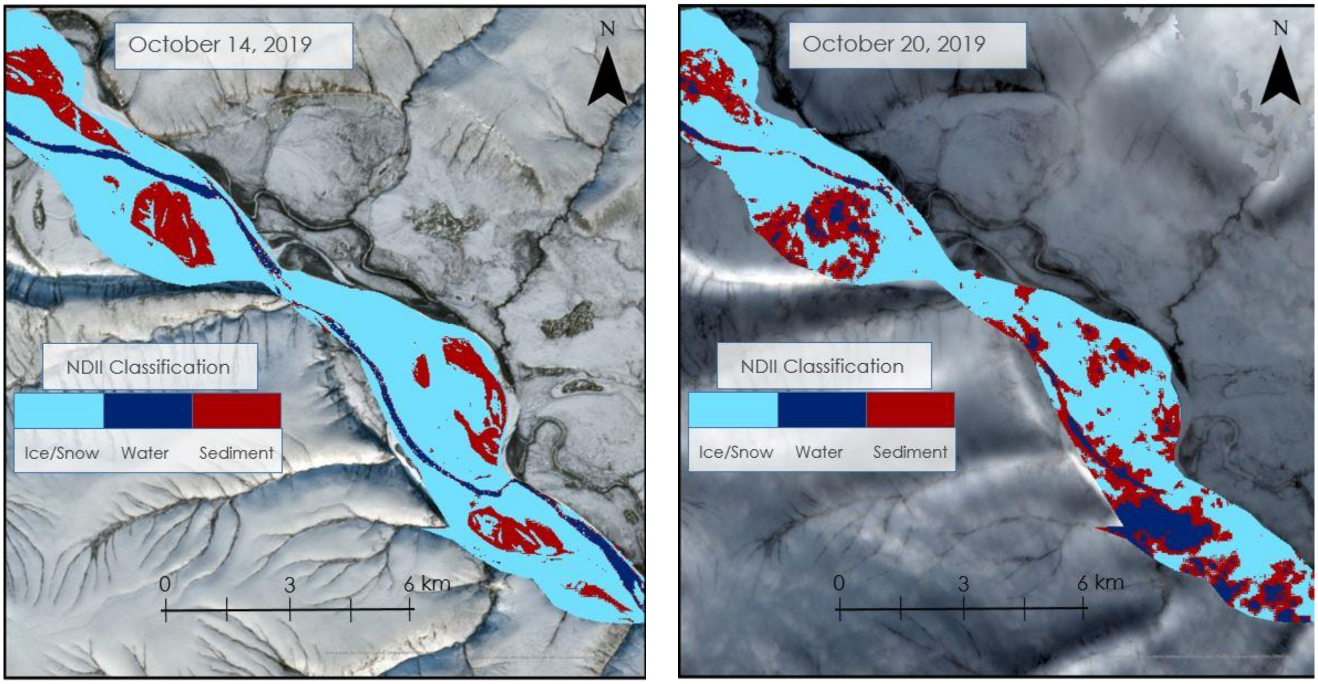

[Basemap Credit: State of Alaska, Esri, TomTom, Garmin, StateGraph, METI/NASA, USGS, EPA, NPS, USDA, USFS, Esri, USGS]

Figure B1. Fall 2019 Time Series Ice Formation Map in Colville River; Oct 14, 2019 (a), Oct 20, 2019 (b).

Appendix C

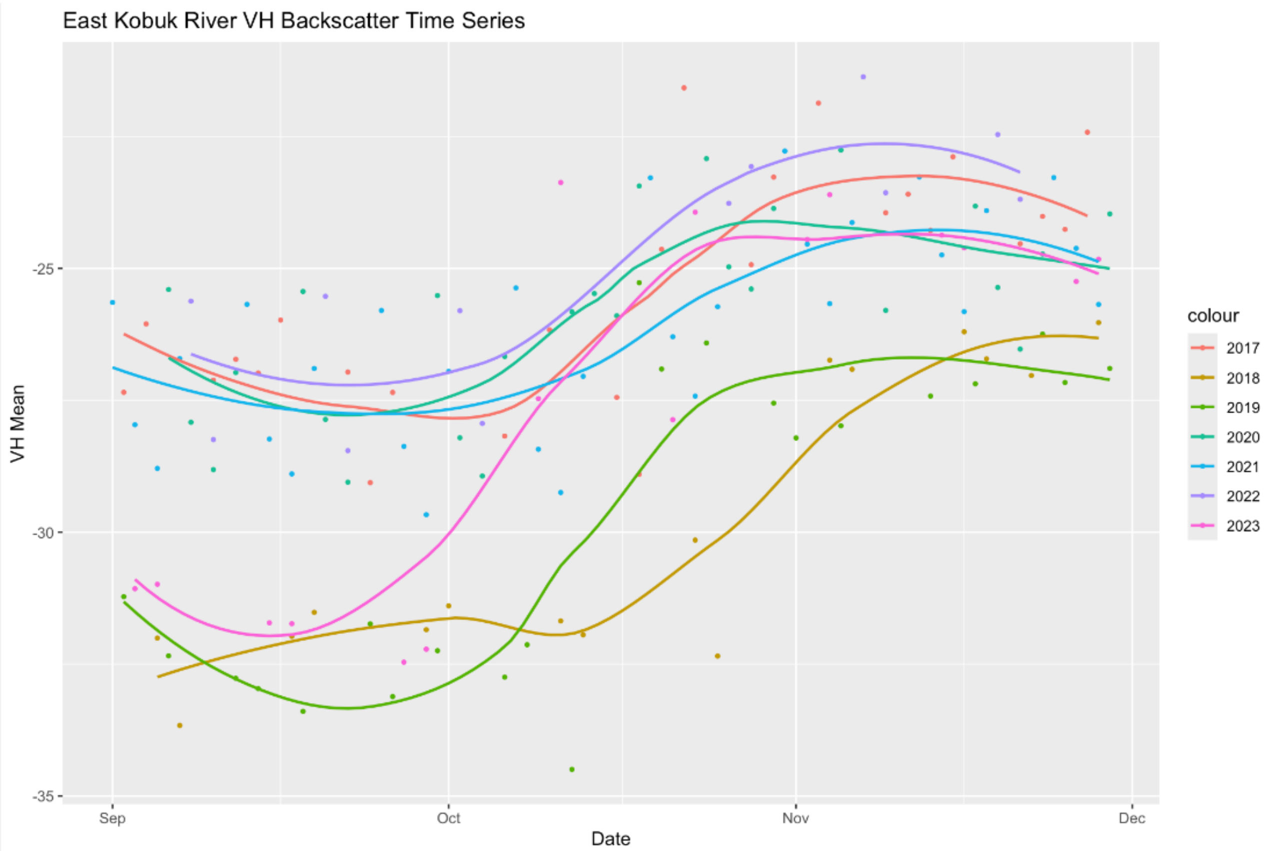

Figure C1. VH backscatter mean by year in East Kobuk.

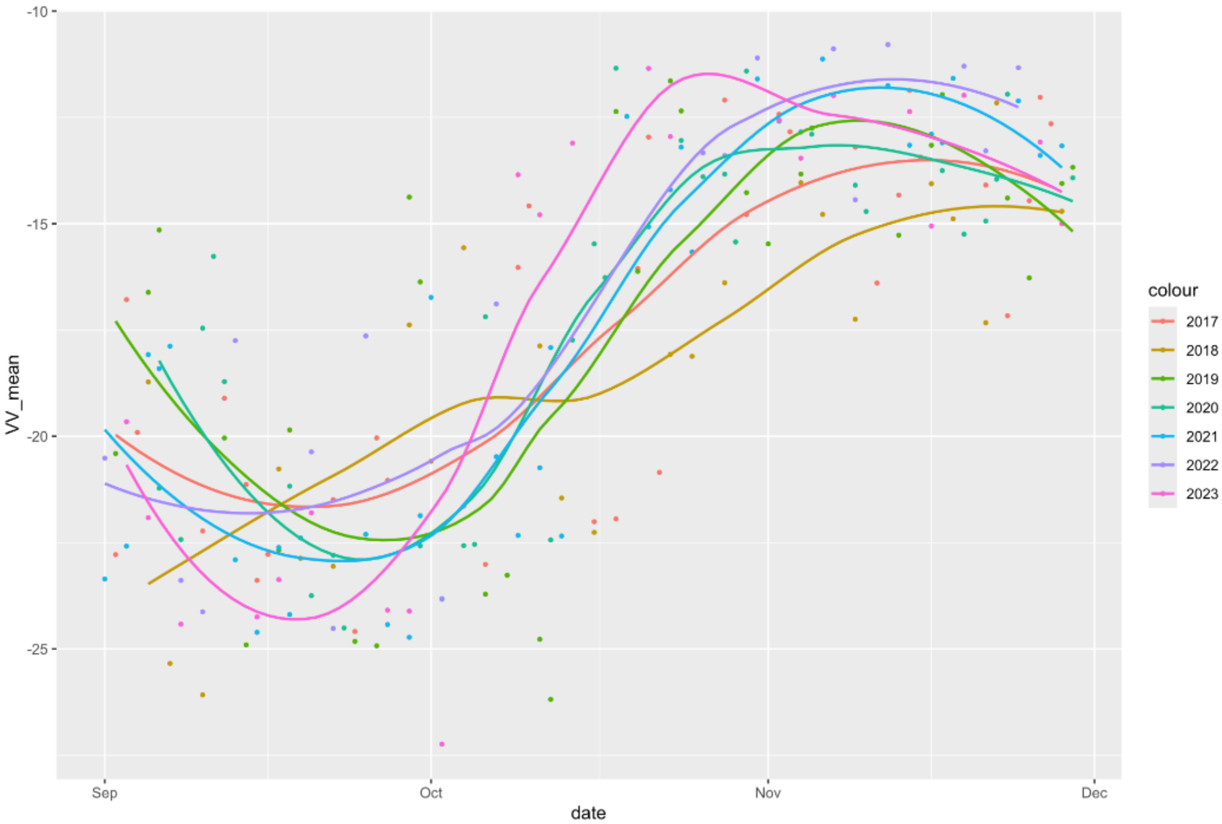

Figure C2. VV backscatter mean by year in West Kobuk.

Appendix D

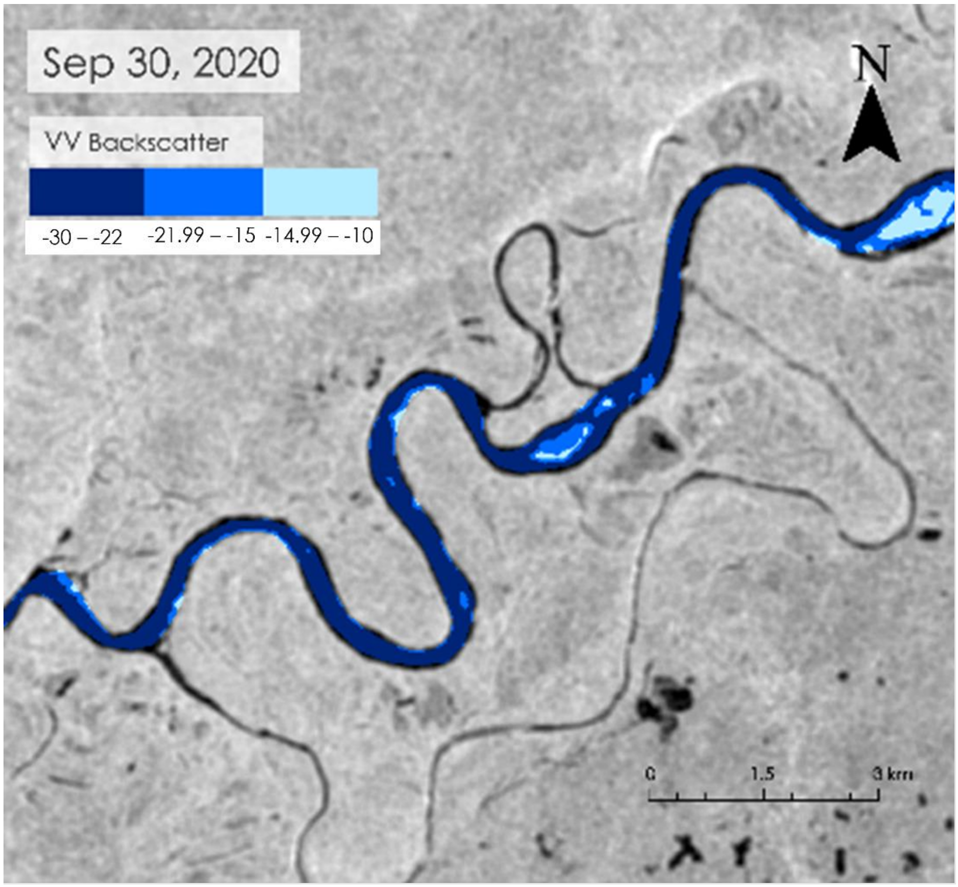

Figure D1a. Fall 2020 Freezing timeline in a section of the West Kobuk River using VV, Sep 30, 2020.

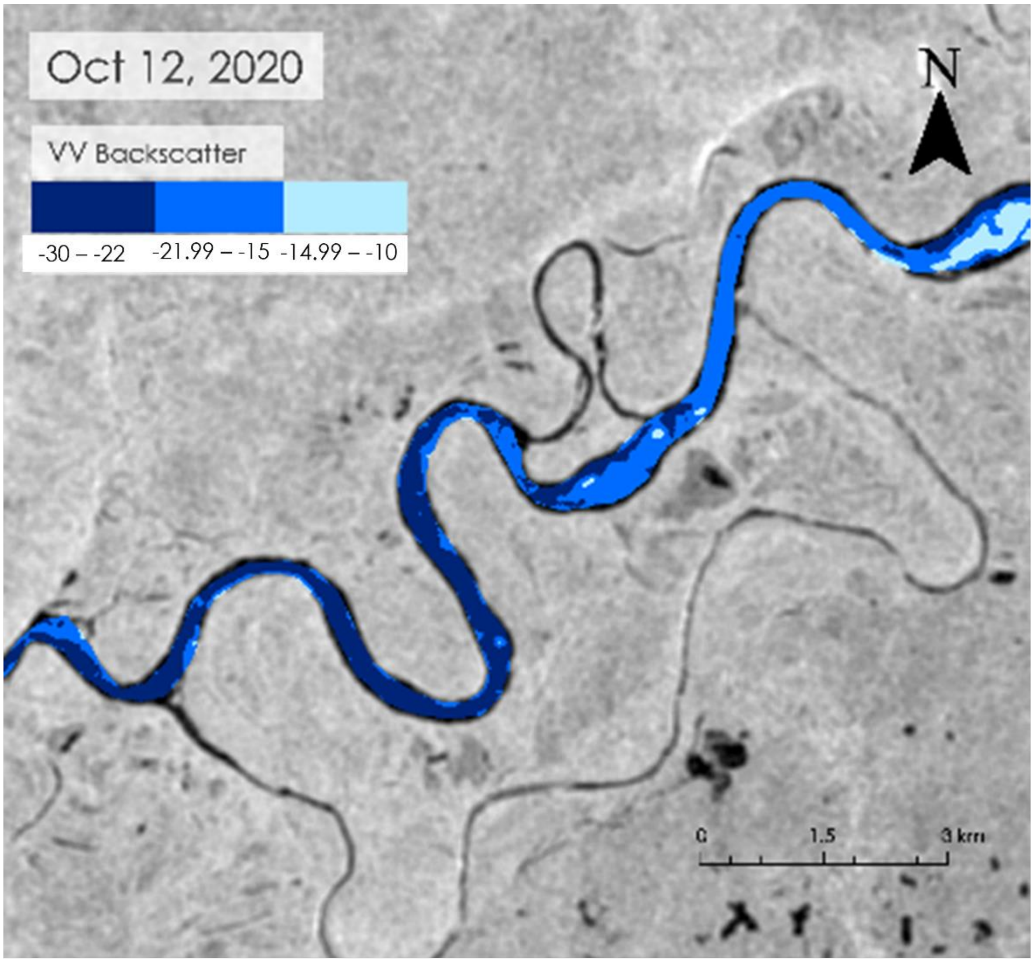

Figure D1b. Fall 2020 Freezing timeline in a section of the West Kobuk River using VV, Oct 12, 2020.

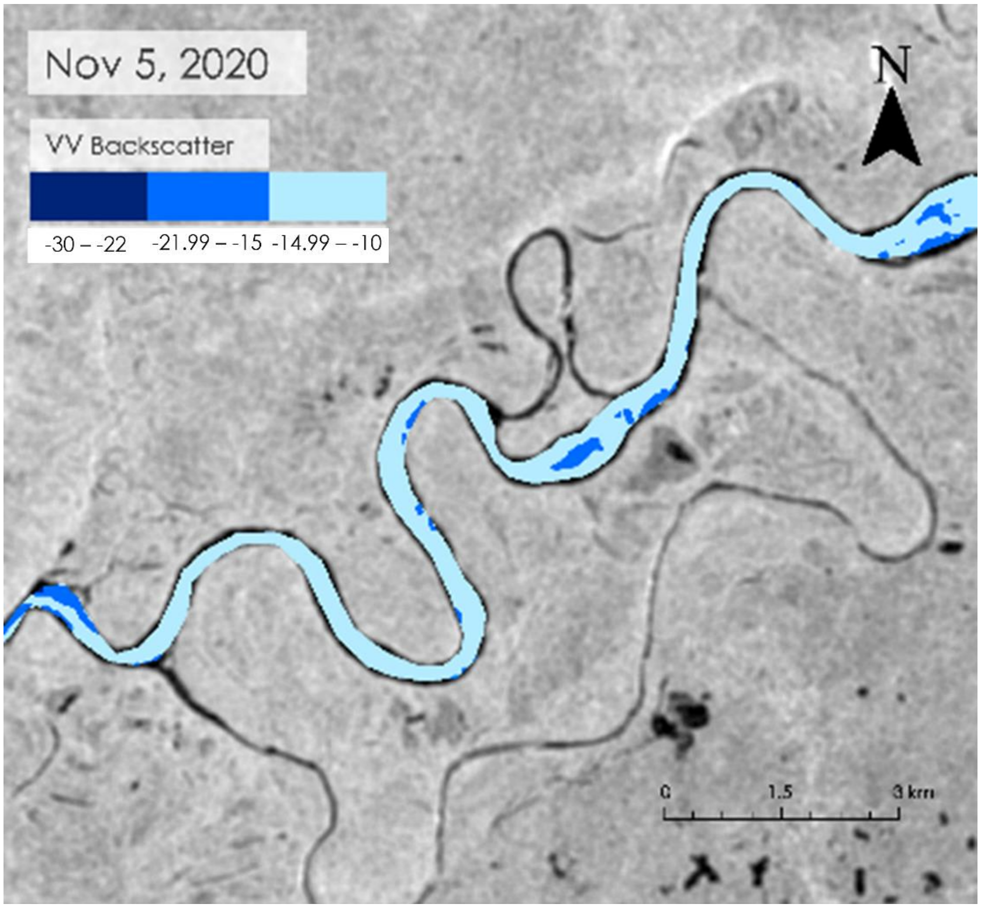

Figure D1c. Fall 2020 Freezing timeline in a section of the West Kobuk River using VV, Nov 5, 2020.

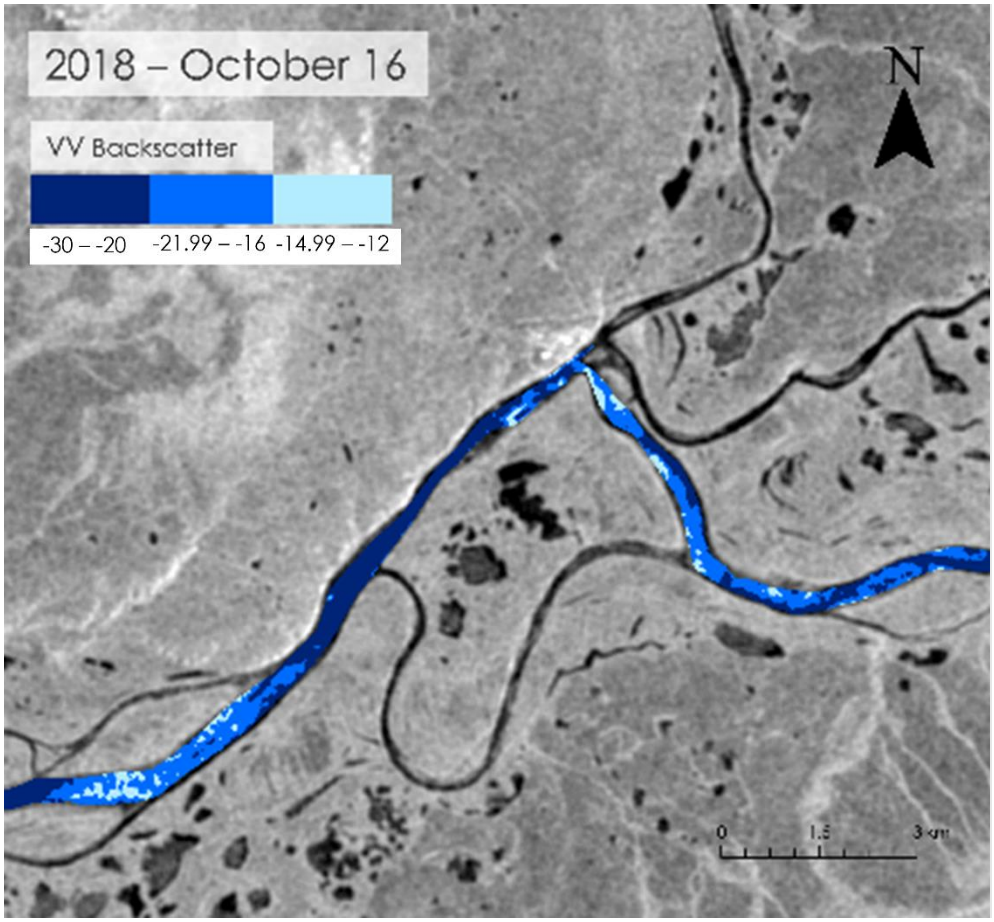

Figure D2a. Mid-October over the years in a section of the West Kobuk River using VV, Oct 16, 2018.

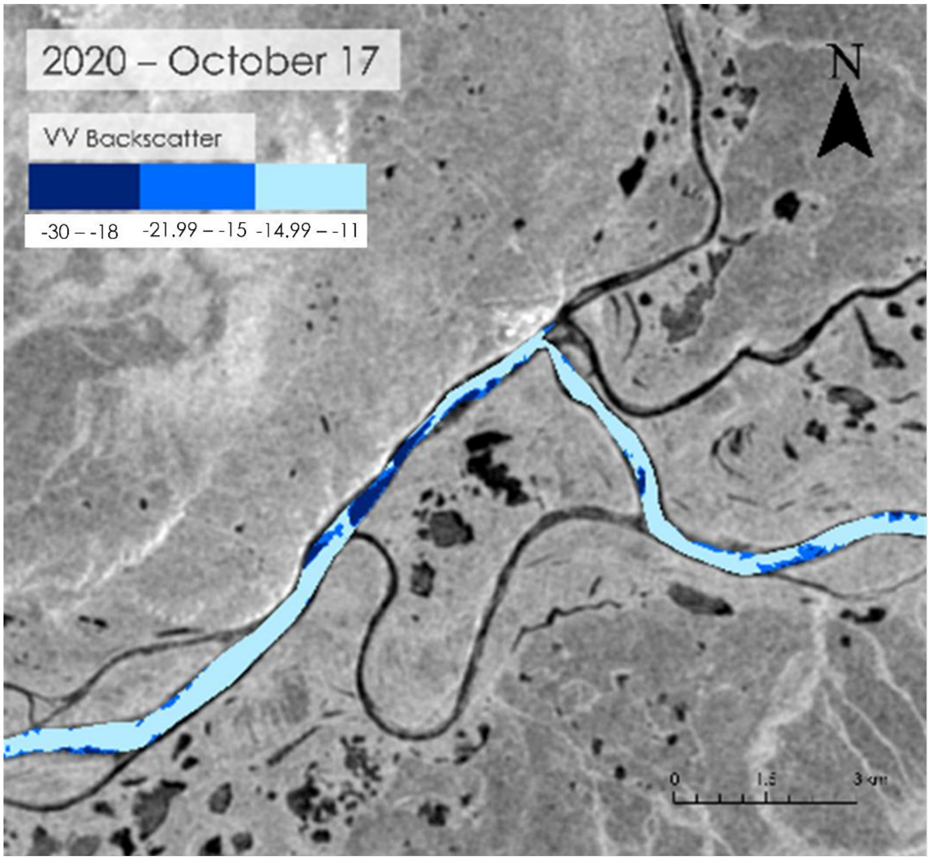

Figure D2b. Mid-October over the years in a section of the West Kobuk River using VV, Oct 17, 2020.

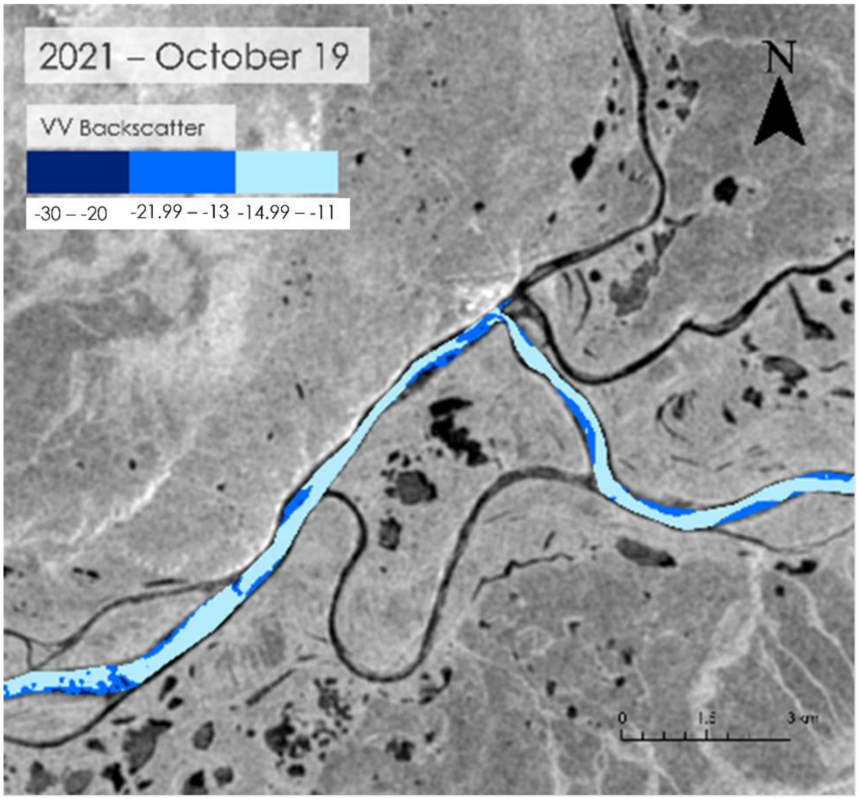

Figure D2c. Mid-October over the years in a section of the West Kobuk River using VV, Oct 19, 2021.

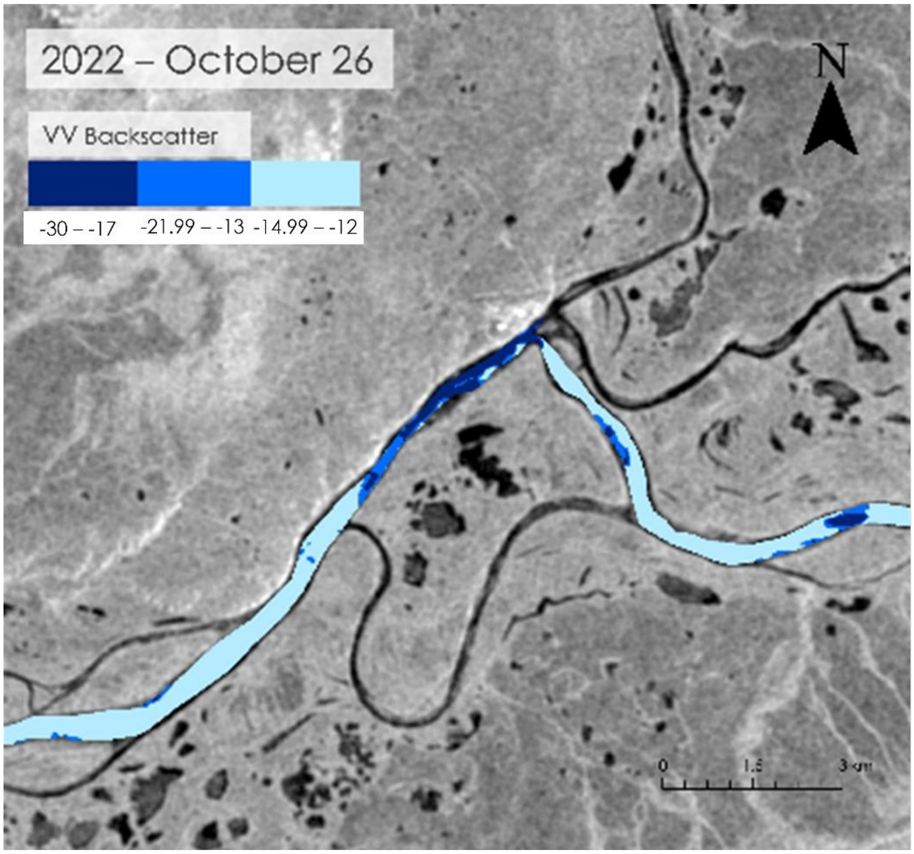

Figure D2d. Mid-October over the years in a section of the West Kobuk River using VV, Oct 26, 2022.

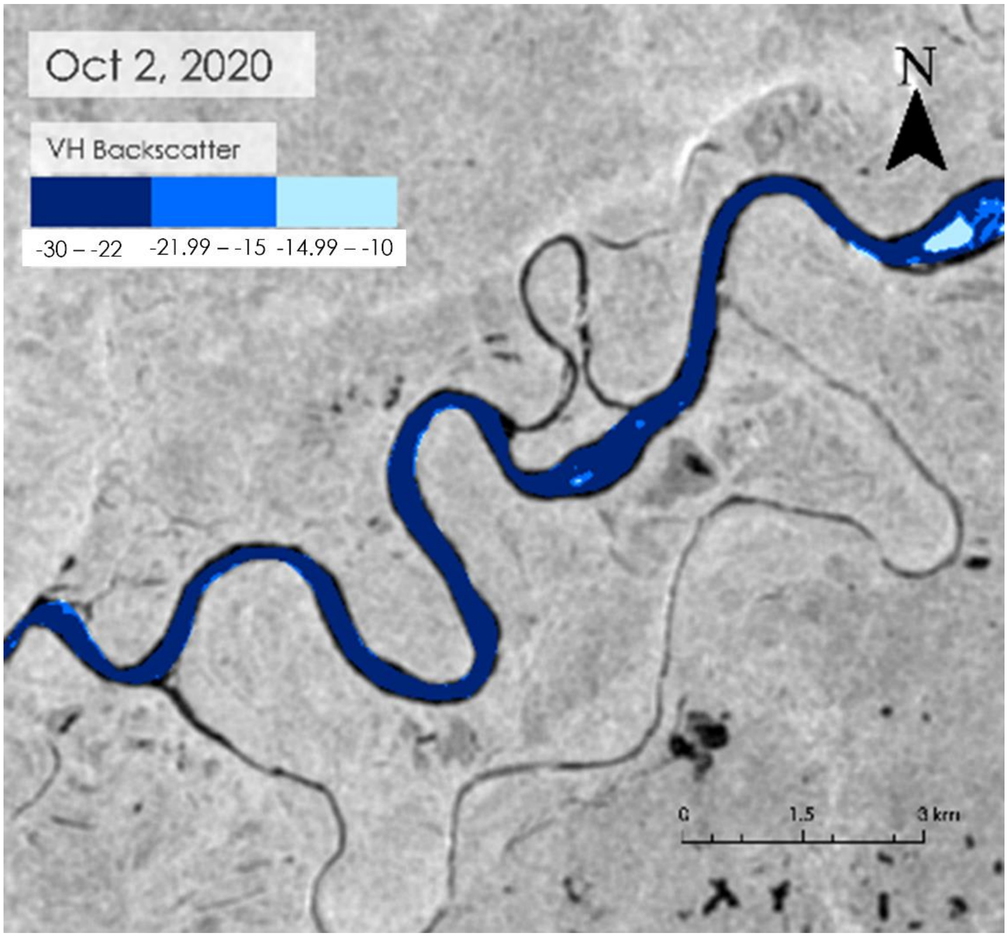

Figure D3a. Fall 2020 Freezing timeline in a section of the West Kobuk River using VH, Oct 2, 2020.

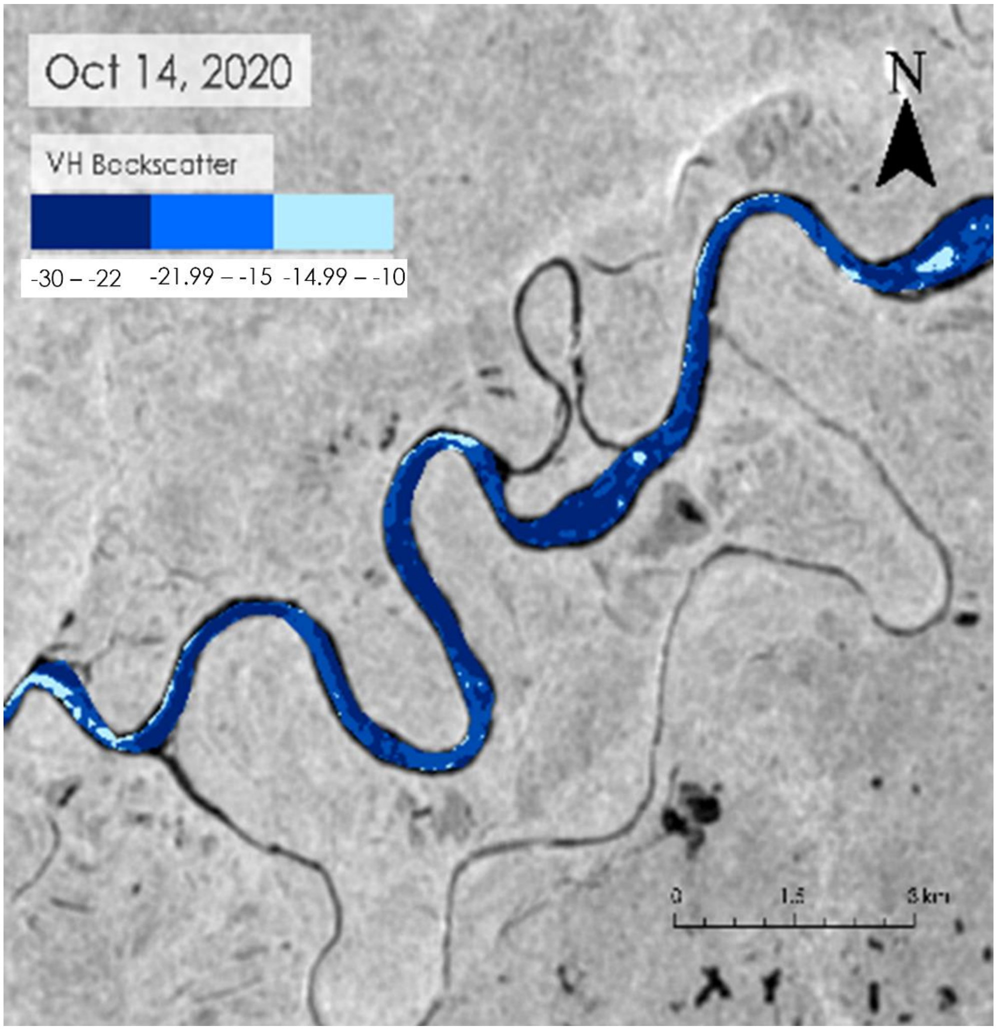

Figure D3b. Fall 2020 Freezing timeline in a section of the West Kobuk River using VH, Oct 14, 2020.

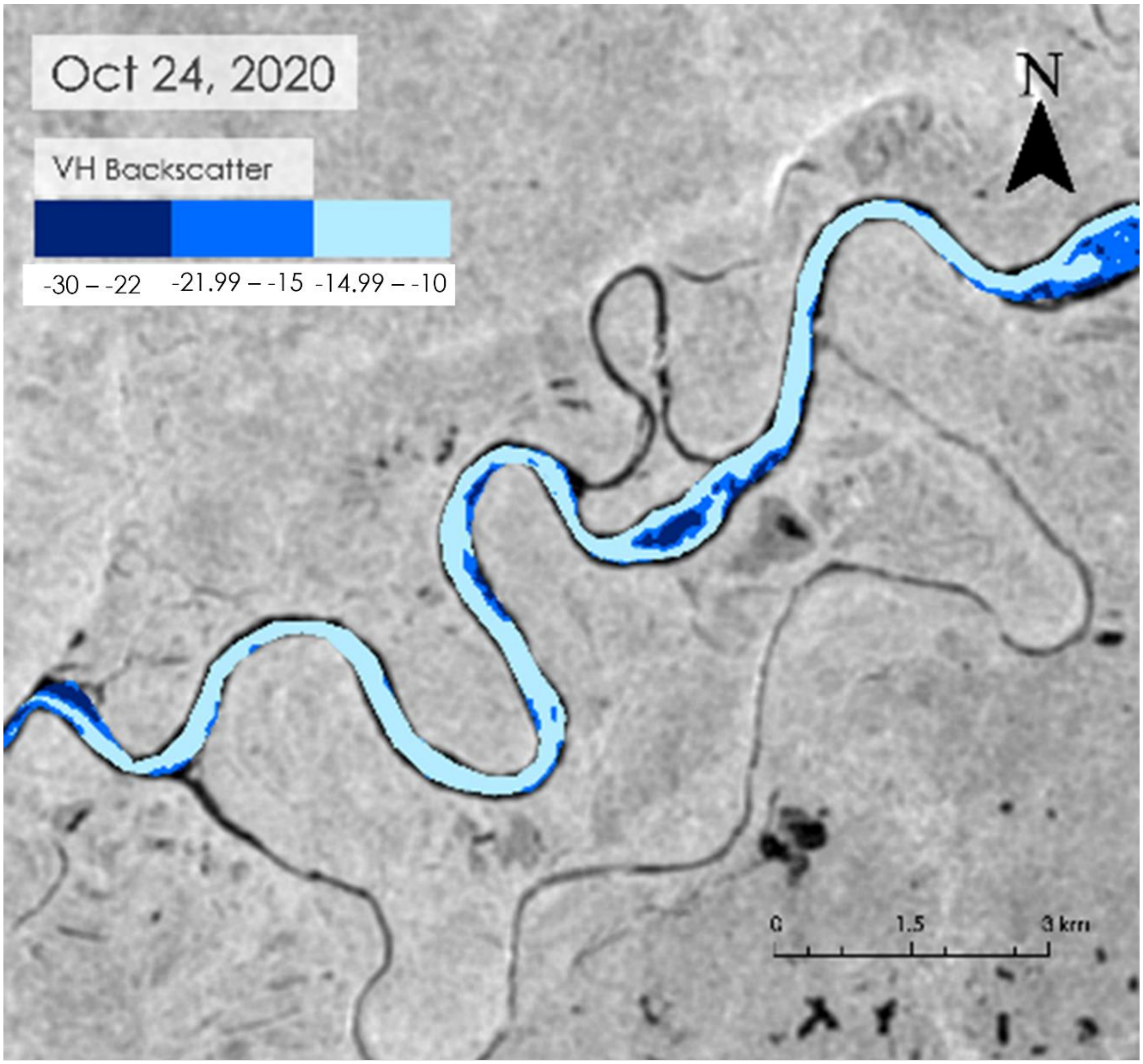

Figure D3c. Fall 2020 Freezing timeline in a section of the West Kobuk River using VH, Oct 24, 2020.

Appendix E

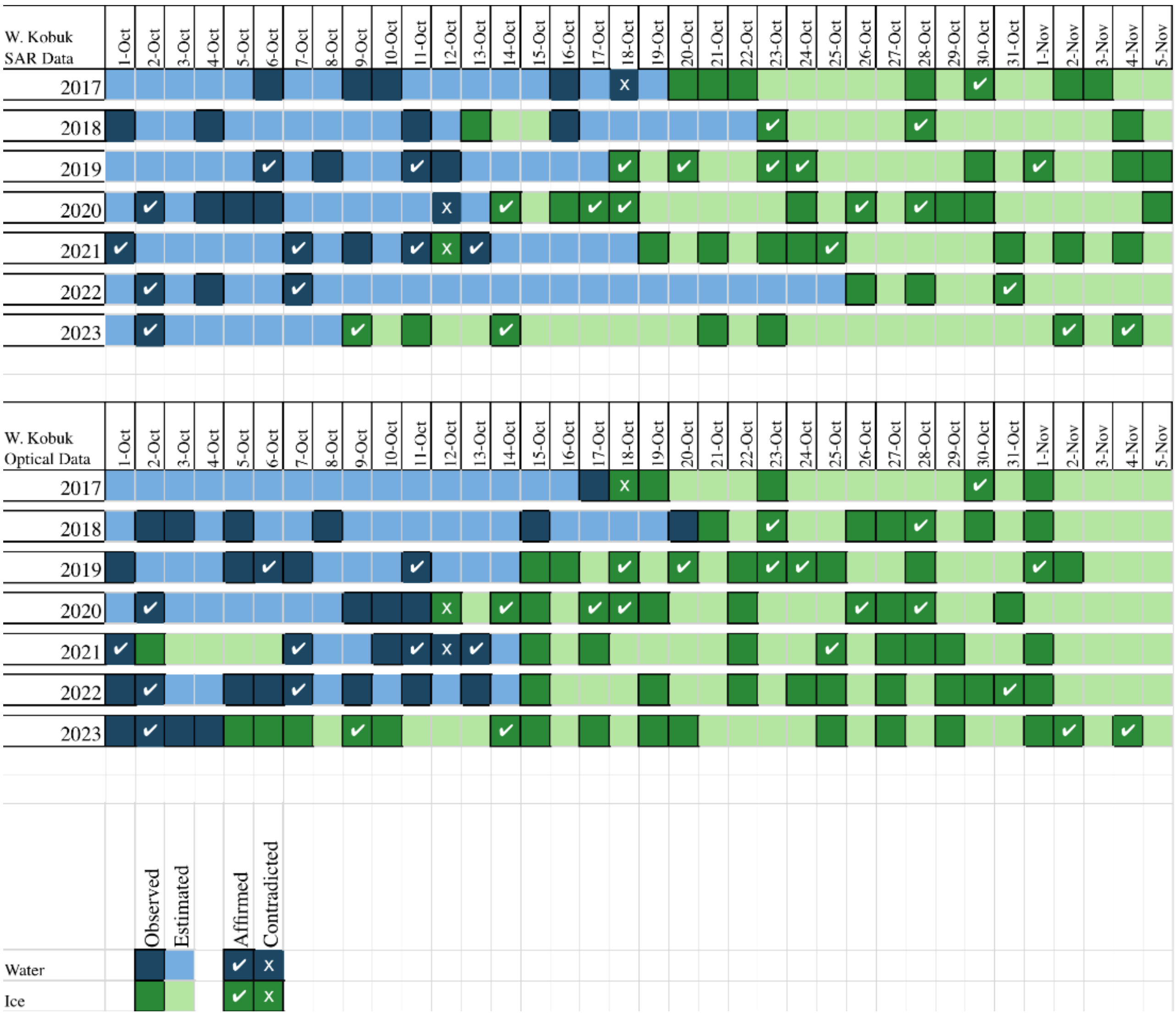

Figure E1. Timeline of yearly freezing dates comparing SAR and optical data.